CARBON MONOXIDE ADSORPTION ON Pt MONOLAYER ON Pd(hkl) SURFACE STUDIED BY SUBTRACTIVELY NORMALIZED INTERFACIAL FOURIER TRANSFORM INFRA-RED SPECTROSCOPY

A Thesis

Presented to

the Faculty of the Department of the Biomedical Engineering

University of Houston

In Partial Fulfillment

of the Requirements for the Degree

Master of Science

in Biomedical Engineering

by

Milan Slavkovic

August 2012

CARBON MONOXIDE ADSORPTION ON Pt MONOLAYER ON Pd (hkl) SURFACE STUDIED BY SUBTRACTIVELY NORMALIZED INTERFACIAL FOURIER TRANSFORM INFRA-RED SPECTROSCOPY

Milan Slavkovic

Approved:

Co-Chair of the Committee
Dr. Stanko R. Brankovic, Associate Professor
Electrical and Computer Engineering

Committee Members:

Co-Chair of the Committee
Dr. Metin Akay, Professor and Chair
Biomedical Engineering

Dr. Ting Y. Chen, Research Assistant Professor
Biomedical Engineering

Suresh K. Khator, Associate Dean
Cullen College of Engineering

Dr. Metin Akay, Professor and Chair
Biomedical Engineering

ACKNOWLEDGEMENTS

I would like to express my deepest appreciation to my thesis advisor, Dr. Stanko R. Brankovic, for his patience, insightful and sincere remarks throughout the research work, and for providing me with a research environment of the highest quality. His continuous motivation has worked as a strong driving force in bringing the best out of me.

I would also like to extend my gratitude to Dr. Metin Akay and Dr. Ting Chen for guiding me thorough the Biomedical Engineering program and classes and helping me throughout the project by serving on my thesis committee. I also take this opportunity to thank all of the members of the Electrochemical Nanofabrication Synthesis Group and in particular Qiuyi Yuan for providing an intellectual laboratory atmosphere. Finally, I am grateful to my loving parents and my older brother who have always been supportive and encouraging to me when I needed them the most.

CARBON MONOXIDE ADSORPTION ON Pt MONOLAYER ON Pd(hkl) SURFACE STUDIED BY SUBTRACTIVELY NORMALIZED INTERFACIAL FOURIER TRANSFORM INFRA-RED SPECTROSCOPY

An Abstract

of a

Thesis

Presented to

the Faculty of the Department of the Biomedical Engineering

University of Houston

In Partial Fulfillment

of the Requirements for the Degree

Master of Science

in Biomedical Engineering

by

Milan Slavkovic

August 2012

ABSTRACT

The progress of our civilization is critically dependent on the discovery of new materials and structures with better properties, novel functionality and applications. The ultra thin metal overlayers represent one class of such structures with increasing application in fuel cells.

In our work, the two-dimensional Pt monolayers on Pd(hkl) were used as model system to study CO adsorption. The Pt_{ML}/Pd(hkl) were obtained using surface limited red-ox replacement reaction of underpotentially deposited Cu monolayers on Pd(hkl) with, and without presence of citrate in the reaction solution. The strength of the CO adsorption on Pt monolayer was studied by subtractevily normalized interfacial fourier transform infra-red spectroscopy (SNIFTIRS). The SNIFTIRS results indicate synergistic effect of both; Pt monolayer and Pd(hkl), yielding a qualitatively new phenomenon where the bond of adsorbed CO on Pt_{ML}/Pd(hkl) is weaker than the corresponding CO bond on each of the bulk metal surfaces. This result has fundamental importance when catalysts for oxygen reduction and hydrogen oxidation reactions are considered where the surface poisoning by intermediates or impurities is responsible for reduced catalyst activity.

TABLE OF CONTENTS

LIST OF FIGURES

LIST OF TABLES

CHAPTER 1: INTRODUCTION

Catalysts are the heart of many chemical and almost all biological transformations of molecules and mixtures to useful products. In terms of chemical conversions, catalysts are heavily utilized for refining, the production of chemicals, polymerization and exhaust emission reduction. Future perspectives of catalyst use include the reduction of pollution from chemical and petroleum processes, electronics manufacturing and pharmaceutical synthesis. However, catalysts are likely to be of main importance in the production of energy necessary to sustain the needs of the fast growing world population. Energy deficiency will likely be a bigger problem than many other social issues such as water and food shortages since a solution for this problem could be used as strategies for others [1]. Specifically, there are big requirements for novel catalytic materials and their use in energy production. Major areas for expected advancement of new material catalyst are: emission reduction of CO_2, development of new photocatalysts for water activation for direct production of hydrogen and oxygen, and development of inexpensive electrocatalysts with improved characteristics for fuel cell deployment.

The modern approach in improving the characteristics of electrocatalysts is to develop a method that can predict catalyst performance (for example density functional theory-DFT calculation) and then use the knowledge to synthetize materials with improved features. The characteristics of improved catalysts should be defined as a function of chemical composition, molecular structure and morphology. The ability to understand the reactive surface on a molecular level has tremendously increased over the past century due to major advances in characterization techniques such as scanning tunneling microscopy (STM), ion scattering spectroscopy (ISS) and infrared spectroscopy

(IRS). Reflection adsorption infrared spectroscopy (RAIRS) is a widely used method for determination of electrochemical reactivity. It provides insights in products and intermediates of reaction which gives more information needed for development of better catalysts.

Dominant criteria in the design of better catalyst material could be narrowed to the development of a highly active catalyst which will produce desirable products while maintaining activity for a prolonged period. The activity is mostly defined as a function of rate-determing step or steps in the overall process in terms of kinetics. The kinetics are further dictated by the nature of interactions between the atoms of catalysts and adsorbate (intrinsic chemical interactions) and the nature of the reaction environment. The environment includes the influence of support, alloy composition and structure, defects, relaxation and reconstruction of the surface, solvent media, etc.

The elementary processes that a catalytic reaction is comprised of can be defined as: chemisorption, dissociation, diffusion, recombination and desorption. Chemisorption is possible when interaction energy of reactants with the surface is strong enough to form chemical bonds between the adsorbate and surface atoms while at the same time weakening the internal bonds within the adsorbate and thus promoting the dissociation process. In order for the adsorbate molecule to decompose it should strongly bind to the surface. Interaction energy has to be strong enough to overcome the internal molecule energy. Hence, when the decomposition is the rate limiting step, the rate should increase by increasing interaction energy. Alternatively, when molecular fragment produced by decomposition strongly bind to a surface, active sites for adsorption of reactants are blocked, making desorption the rate limiting step. In that case, increasing interaction

energy will have the opposite effect of decreasing catalyst performance. This leads to the calculation of the optimum of adsorbate-catalyst surface interaction strength in order to activate a reaction without poisoning the surface. This balance known as the Sabatier principle, serves as a foundation for the volcano-type plots of catalysts materials for particular reaction (Figure 1-1.).

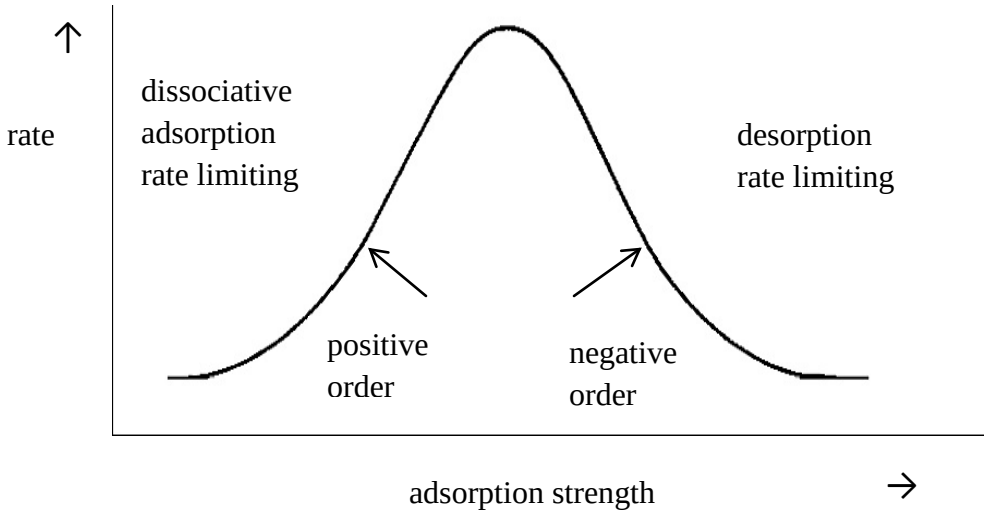

Figure 1-1. Catalytic rate dependence of the adsorption strength.

The plots are made by comparing different catalyst material for same reaction by measuring reactant-adsorption energies and catalytic rate. If the rate increases with increasing adsorption energy, it is positive order of reaction. If it decreases, it is a negative order of reaction. The reaction is considered zero order on the top of the volcano plot, which should coincide with the optimum i.e. maximum rate for the catalyst for that particular reaction. Sabatier-type volcano plots have been constructed for a number of different commercially relevant systems [2]. This kind of plot is widely used in fuel cell research especially when methanol and hydrogen are considered as a fuel. The problem with methanol is the decomposition intermediate CO which strongly adsorb on the

catalyst surface blocking active sites for adsorption of reactants slowing down the process. When considering hydrogen as a fuel, the problem is actually on the cathode side where the OH, in the process of oxygen reduction, can strongly bond to active sites making desorption the rate limiting process. The corresponding volcano plot for this reaction is given in Figure 1-2 [3].

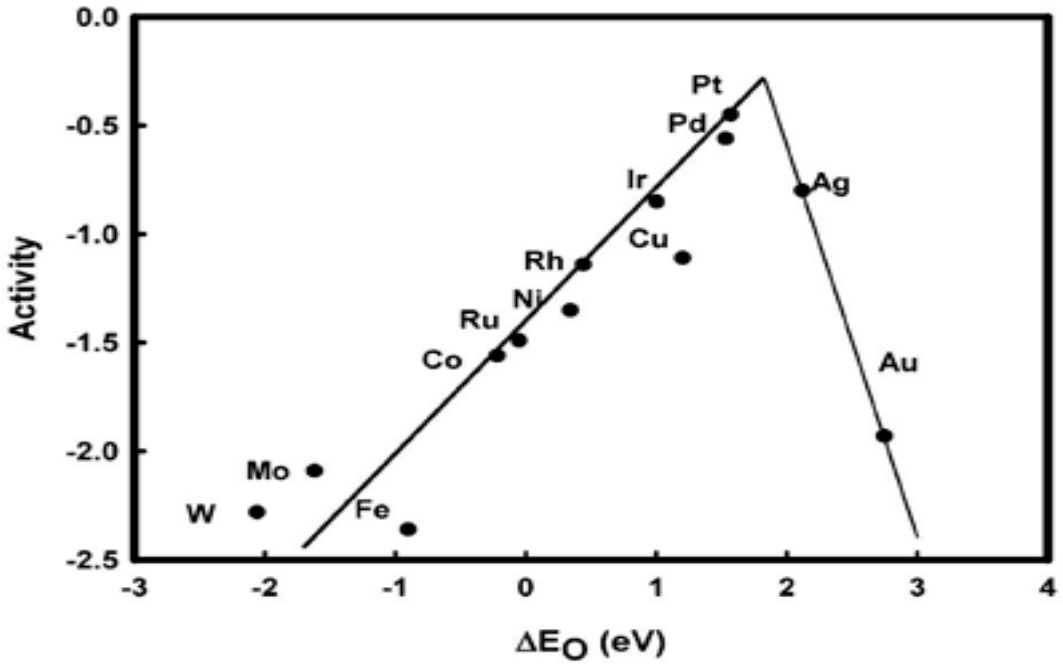

Figure 1-2. Volcano plot of the measured catalytic activity of the oxygen reduction reaction for various transition metal electrodes as a function of the calculated binding energy of oxygen atoms (adopted from reference [3]).

Clean platinum is one of the most frequently used catalyst material and for a long time was considered the best catalyst for oxygen reduction. The main problem with platinum, aside from OH poisoning, is high cost. The efforts for solving these problems were made by Pt alloying with transition metals or by decreasing the Pt loading by decreasing particle size with some improvements but not entirely satisfactory [4].

A promising approach to solve the problem of high Pt content and low efficiency is the Pt-monolayer model; the primary aim of this work. The idea is to fine “tune” metal catalysts which are near the top of the volcano plot by promoting metal-support interaction via electronic or other effect to increase performance for a particular reaction, i.e. oxygen reduction. As such, methods of adsorption of well-ordered metal atomic layers onto a foreign metal substrate have attracted the attention of the scientific community. This can be done by underpotential deposition i.e., process occurring at potentials more positive than reversible potential for specific reaction. Furthermore, more noble metal can be used for the surface-limited redox replacement (SLRR) of sacrificial less noble underpotentially deposited metal layer at open circuit potential (OCP). Deposition is irreversible and amount of deposited noble metal is controlled by stoichiometry of the redox replacement reaction [5].

It has been well established that combined action of two metals can alter electrochemical reactions [6]. There are several different effects of action of the cocatalysts related to the assembly and type of interactions of metal-metal systems. These include geometric (ensemble) effects, electronic (ligand) effects, strain effects and bifunctional effect (Figures 1-3). The geometric effect is related to requirement of more than one site to be active for adsorption process of particular molecule. The example is adsorption of methanol on Pt surface which require three to four Pt atoms [7]. In the ligand effect, is when the electronic properties of the substrate or primary metal are modified by the other material (i.e. secondary metal) in a way that either the adsorption energy is modified or the activation energy is changed. The electronic effect is explained by the direct influence of second component on the electronic states of the first metal and

vice versa (true electronic effect) [7]. The strain effect is due to strain exerted by the second metal on the primary metal caused by a mismatch in lattice constants between these two metals in overlayer configuration. The mismatch causes broadening and lowering (or narrowing and increasing) of the energy of the *d*-band of the primary metal.

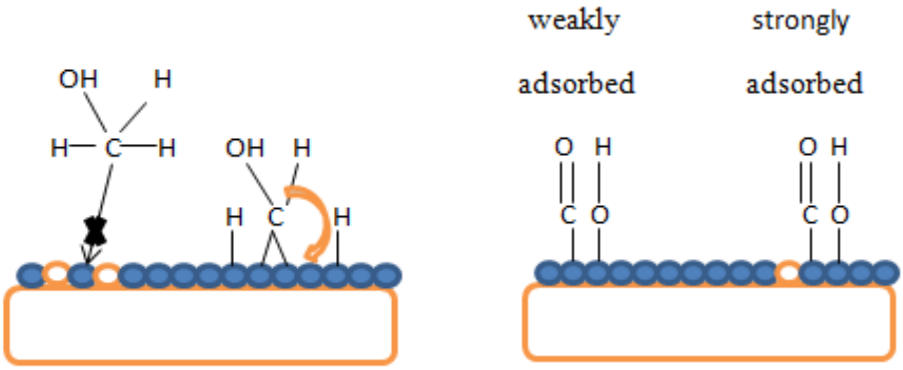

a) b)

Figure 1-3. Sketch of mechanism of action of cocatalysts (white spheres): (a) ensemble (geometric effect) and (b) ligand (electronic) effect.

The best model to explain bifunctional mechanism is anodic oxidation of CO molecule by stripping voltammetry. The most explored surfaces for studying CO oxidation are Pt, Ru, Sn and their alloys. After CO is adsorbed at a specific potential (around 0 V vs RHE) the characteristic current density (j) – potential (V) curve can be obtained for CO oxidation [6]. Oxidation currents of CO on Ru have the onset and stripping peak at more negative potential than a Pt surface. This correlates to adsorption of oxygen containing species at more negative potential onto Ru electrode. The oxygen-containing species are needed for electrooxydation of CO by the mechanism:

$$Ru + H_2O \rightarrow (OH)_{ads} + H^+ + e^- \quad , \qquad (1\text{-}1)$$

$$(CO)_{ads} + (OH)_{ads} \rightarrow CO_2 + H^+ + e^- . \quad (1\text{-}2)$$

The alloy surface made by combination of these two metals showed different behavior for CO oxidation depending on the percentage of the Ru in the RuPt alloy. The stripping peaks are shifted more negatively for the 0.07, 0.33 and 0.46 percent of Ru content. Activity related to the enrichment of the alloy with Ru plateaus at around 50% Ru to Pt [6]. The reason for the increased activity of the bimetallic alloy surface can be explained by a bifunctional mechanism in which Ru atoms serve as nucleation sites for adsorption of oxygen-containing species which then react with CO adsorbed either on a Pt or a Ru site nearby. When compared with the oxidation of CO as a dissolved gas on the same surfaces, similar behavior of continuous oxidation to anodic stripping occurs. The main difference is due to the onset of continuous oxidation shifted to higher potentials. This behavior is considered as a non-bifunctional mechanism due to competition of COads and OHads for the same adsorption sites [6]. In this case, the negative reaction order occurs because the rate determining step is a reaction of both surface adsorbed reactive species. Both species compete for the same sites and there is stronger adsorption of one reactant (CO). An alloy which is considered truly bifunctional is PtSn. PtSn exhibits a positive reaction order which infers an absence of competition between OHads nucleation on Sn and CO adsorption at Pt sites. The negative shift of the onset potential for this system compared to RuPt confirmed the high activity of the alloy. Furthermore, the high activity of the PtSn alloy can be attributed also to weakly CO bonding, i.e. CO is highly mobile and reactive on the surface which is a consequence of intermetallic bonding between Pt and Sn atoms i.e. electronic effect [6].

Voltammetric profiles of carbon monoxide oxidative desorption are widely used for the analysis of the catalyst performance of bimetallic surfaces with respect to adsorption and oxidation reactions. Carbon monoxide is used as a probe molecule due to its behavior as a prototype adsorbate, a surface poison and an intermediate in reactions with small organic molecules (methanol, ethanol, formic acid, etc.). Hence, further research of the oxidation of CO may facilitate the understanding of the oxidation processes.

Furthermore, the behavior of adsorbed CO on catalyst surface, such as site occupation, crystallographic surface dependence and potential dependence, gives more insight of the characteristics of the designed catalyst. *In-situ* infrared spectroscopy is typically used to deliver qualitative and quantitative data of the electrochemical processes on catalysts with CO as a probe molecule. There are diverse array of IR techniques which can be used to describe the behavior of adsorbed CO. In this work focus is on SNIFTIRS (Subtractively Normalized Interfacial Fourier Transfrom Infrared Spectroscopy) on Pt and Pd surfaces. The CO binds strongly on the transition metals. The binding mode of CO as a diatomic molecule consists of CO-to-metal σ- donation and metal-to-CO π^*-back donation. A sigma bond (σ) is formed when a nonbonding electron pair of carbon donates an electron to an empty σ orbital of a metal. Together with this process there is release of electrons from d-orbitals of the metal into empty π-antibonding orbitals of the CO. As a consequence of synergistic bonding, the metal-carbon bond is strengthened, while the carbon-oxygen bond is weakened. The weakening of the CO bond is most readily detected by vibrational spectroscopy, where νCO, the stretching frequency, is found to be very sensitive to changes in the CO-bond caused by backdonation. Hence, if negative

potential is applied, the electron density on the electrode will be higher, promoting π^*-backbonding and decreasing C-O bond strength i.e., decreasing the vibrational frequency which is obtained from infrared spectra. As such, the CO-metal bond strength will increase upon application of negative potential.

The unique properties of CO can be used for characterizing the catalyst i.e. stronger or weaker bonded molecules will exhibit a corresponding shift in frequency response. Examination of the frequency response shifts can provide information on the catalyst's ability to maintain maximum activity for a specific reaction. Comparison with other catalysts and confirmation of the trends of catalytic behavior of a novel catalyst can be obtained using plots of peak position as a function of applied potential. Such plots are a graphical representation of the influence of electrical field on the electrons participating in metal-CO bond (Stark effect).

CHAPTER 2: SUBTRACTIVELY NORMALIZED INTERFACIAL FOURIER TRANSFORM INFRARED SPECTROSCOPY (SNIFTIRS)

In the past decades various surface techniques are studied to gain useful information about surface structure (physical and electronic) and composition (chemical). The basic probes that could be applied to the surface include electrons (Auger electron spectroscopy-AES, scanning electron microscopy-SEM, low energy electron diffraction-LEED, etc.), ions (ion scattering spectroscopy-ISS, secondary ion mass spectrometry-SIMS, etc.), photons (X-ray photoelectron spectroscopy-XPS, infrared spectroscopy-IR, etc.), electrical field (scanning tunneling microscopy-STM, etc.) … Due to technological breakthroughs, such as the advent of Fourier transform infrared spectroscopy-FTIR, the range of applications of vibrational spectroscopies has increased enormously owing to its increased sensitivity, speed, accuracy and stability. Among the other classes of vibrational spectroscopy techniques (Raman spectroscopy, sum frequency generation (SFG)) infrared spectroscopy (IR) can be considered as general tool for interfacial studies at present [8]. Various infrared techniques provide the most definitive means for *in-situ* characterization of interfaces on a molecular level. Which technique is chosen depends on what information is wanted from the system under the study. The new applications which uses infrared spectroscopy are related to the study of adsorbed ions [9], reaction on bimetallic surfaces [10], nanoparticle catalyst [11], properties of fuel cell membrane [12] and organic films [13].

The technique widely used for characterization of adsorbates on surface of catalysts is reflection-adsorption infrared spectroscopy (RAIRS). Due to high reflectivity from metal single crystal surface of the catalyst and since the technique is optical

(photon), detected signal is sufficient to provide information needed, especially in ultra-high vacuum (UHV) system. The use of RAIRS in electrochemical environment is more difficult due strong absorption of infrared radiation by water. There are two main approaches to overcome this problem. One is related to deposition of thin metallic (or other material under study) film as working electrode on the surface of infrared optical window (usually Si or Ge hemisphere). The penetrating infrared wave thorough the film to the layer of adsorbates is exempt of interference from infrared absorption from bulk water. Another positive effect of this system is enhanced infrared absorption of adsorbates on metallic film, so-called surface-enhanced infrared absorption (SEIRA) effect. The main limitation of this technique is stability of the thin film (thicknesses around 20 nm) and control of the surface structure [14].

The other approach for the *in-situ* infrared characterization of the electrode-solution interface is thin layer configuration. This configuration is comprised of reflective surface of a bulk electrode pressed against an infrared window in such way that the thickness of solution layer sampled by infrared radiation is reduced to few microns. This allows the spectroscopic detection of species, intermediates and reaction products within the thin layer. However, even the interference of the bulk electrolyte is reduced tremendously it's still highly influences the sensitivity of the collected spectra. Possible modifications for background correction can be made either by polarization modulation (PM FTIRRAS) or by potential modulation- subtractively normalized interfacial Fourier transform infrared spectroscopy (SNIFTIRS). The first technique uses modulation of p- and s-polarized beam of infrared light to obtain the sample spectrum (p-polarization) and background spectrum (s-polarized). The property of two orthogonal projections of the

electrical field, perpendicular (s-polarization) and parallel (p-polarization) to the plane of propagation of the infrared beam, to form destructive (almost vanishes) and constructive (enhanced) interference on the metal surface, respectively, are foundation of this process [15].

During the second method (SNIFTIRS) the electrode potential is modulated between values E_1, sample potential (usually potential for strong adsorption of probe molecules or production of intermediates) and E_2, background potential (where the reaction is completed or there is no adsorption of probe molecule). The spectrum is obtained by equation:

$$\frac{\Delta R}{R} = \frac{R(E_2) - R(E_1)}{R(E_1)}, \qquad (2\text{-}1)$$

here, the difference between two single beam reflectivities (R) at applied potentials E_1 and E_2, is ratioed to the reflectivity at one of the applied potentials (E_1). The goal of computing this difference (normalized) spectra is to obtain spectra essentially free from bulk contribution. SNIFTIRS method is the part of the external reflection configuration used to study structural aspects of the adsorption processes (Figure 2-1) [16]. A main concern on reducing the background absorption by reducing the thickness in this system is restriction of the mass transport in thin layer which can be a serious drawback for some experiments. Furthermore, complete removal of solution background is not easy in practice. To improve sensitivity and signal to noise ratio (SNR) the system can be adjusted to produce attenuated total reflectance (ATR) on the phase boundary (12) (Figure 2-1). ATR depends on refractive indices of the prism and electrolyte layer and incident angle. If a beam of infrared radiation strikes the interface of two media of

refractive indices n_1 and n_2 from the side of the prism (n_1) at any angle greater than critical angle (θ_c), it is totally reflected and a standing wave is established at the prism-electrolyte medium (boundary 12) [16].

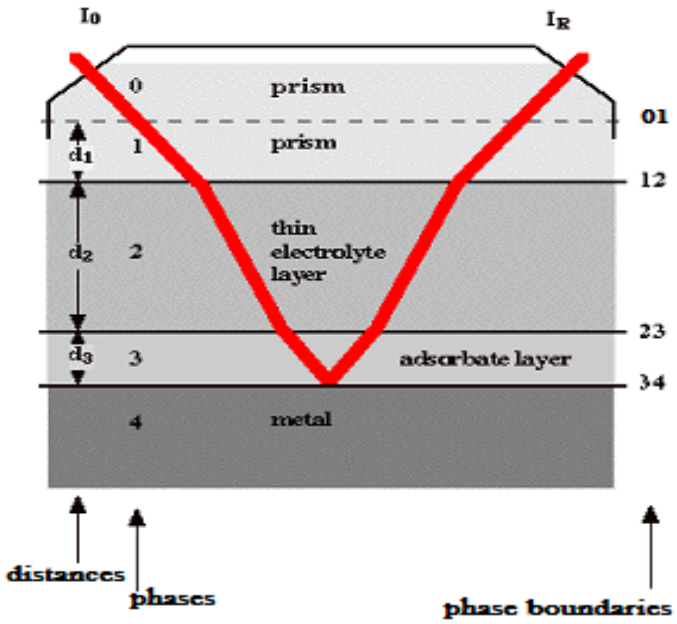

Figure 2-1. Scheme of the SNIFTIRS experiment and multilayer configuration (adopted from reference [16])

Penetration of this beam "into" the thin electrolyte layer and further to adsorbate layer is finite amount with each possible reflection along the boundary via the so-called "evanescent" wave [17].

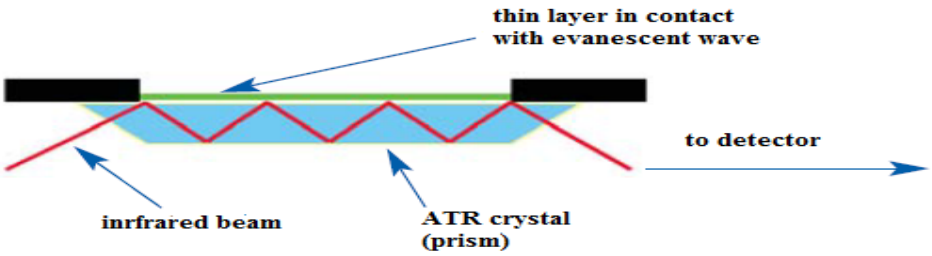

Figure 2-2. Reflection (multiple) ATR system

At the output end of the crystal, the beam is directed out of the crystal and back into the normal beam path of the spectrometer (Figure 2-2.). Term “evanescent “explains its exponential decaying nature which is given by depth of penetration:

$$d_p = \frac{\lambda}{2\pi} (\sin^2\theta - n_{21}^2)^{1/2} \quad , \tag{2-2}$$

where d_p is depth at which the intensity is reduced to 1/e (37 %) of its original value, θ is angle of incidence and n_{21} the ratio of refractive indices of the electrolyte (n_2) and prism (n_1). The critical angle (θ_c) is a function of the real parts of the refractive indices of both the electrolyte and the ATR crystal (prism):

$$\theta_c = \sin^{-1}\left(\frac{n_2}{n_1}\right) \quad , \tag{2-3}$$

With the increase of θ, the penetration gets smaller and approaches 0.1λ at the grazing incidence (θ=90°) for high index media. Thus, fine tuning of the angle is function of the ratio of refractive indices of the material of the prism and electrolyte is needed for maximum IR cross section of adsorbate layer.

CHAPTER 3: UNDERPOTENTIAL DEPOSITION (UPD) AND SURFACE-LIMITED REDOX REPLACEMENT REACTION (SLRR)

The emerging needs for the new energy sources and global progress in the manufacturing industries are greatly conditioned by development of new materials to give better performance. The synthesis of catalyst material with novel functionality and application plays significant role. Further advance of fuel cell technology depends on enhancements of electrocatalytic reaction on surfaces of used catalysts. The idea of improving catalyst performance is generally by modification of their structural and electronic properties. The alteration done on metallic type of electrocatalyst is alloying or surface modification by the deposition of a second metal. The most straightforward method of preparing bimetallic electrodes for fundamental studies is by metallurgic alloying. After development of ultra-high vacuum (UHV) surface analysis techniques, more homogenous and high quality preparation and analysis of alloys is enabled [18]. However, electrochemical deposition techniques go beyond UHV techniques in terms of speed, control of the amount of deposited metal and high pressure environment.

The phenomenon of electrodeposition of a metal on a foreign metal at potentials more positive than the equilibrium potential of the deposition reaction had attracted attention of scientific community due to its potential applications. Such a process is energetically unfavorable and it can occur only because of a strong interaction between the two metals, with their interaction energy changing the overall energetics to favorable forms. Hence, underpotential deposition (UPD) is potential-dependent adsorption of metal atomic layers onto foreign metal substrate at a potential more positive than their reversible potential $E_{M^{n+}/M}$ (E_{rev}) given by *Nernst* equation:

$$E_{M^{n+}/M} = E^{o} + \frac{RT}{nF} \ln a_{M^{n+}} \quad , \tag{3-1}$$

here E° represents the equilibrium (reversible) potential of the electrode surface at standard conditions, R is the universal gas constant, F is Faraday's constant**,** and T is the absolute temperature. The term $a_{M^{n+}}$ represents the activity of the metal ions in solution with n being their oxidation state. Many electrochemical systems that include a metal electrode in solution with different metal ions exhibit an underpotential deposition phenomenon (UPD). More negative potential (E) applied to the metal electrode ($\eta = E - E_{M^{n+}/M} < 0$) is required for the bulk deposition and electrode is at overpotential conditions (η) (Figure 3-1). In the region with positive overpotential the system is at underpotential ($\Delta E = E - E_{M^{n+}/M} > 0$) and metal dissolution ($M \rightarrow M^{n+} + ne^{-}$) takes place.

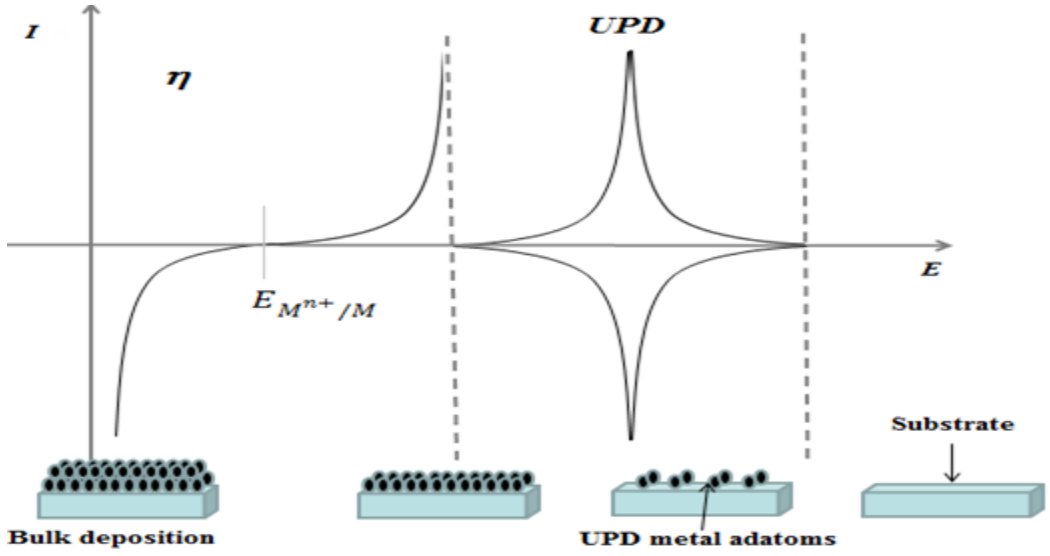

Figure 3-1. Schematics of underpotential deposition.

The UPD is demonstrated by formation of one or two monolayers (MLs) onto a foreign metal electrode. During the UPD process bonding between adatoms and the substrate controls the growth characteristic. The metal ions are reduced through a controlled potential. The characteristic voltammetry features associated with UPD process are typically demonstrated by existence of one or more deposition (stripping) peaks in the underpotential region observed during the potential sweep in cathodic (anodic) direction (Figure 3-2) [19]. For example, the application of the certain underpotential on the electrode surface results in the deposition of the full Cu UPD ML, partial Cu UPD monolayer and free Au(111) surface as indicated in the Figure 3-2.

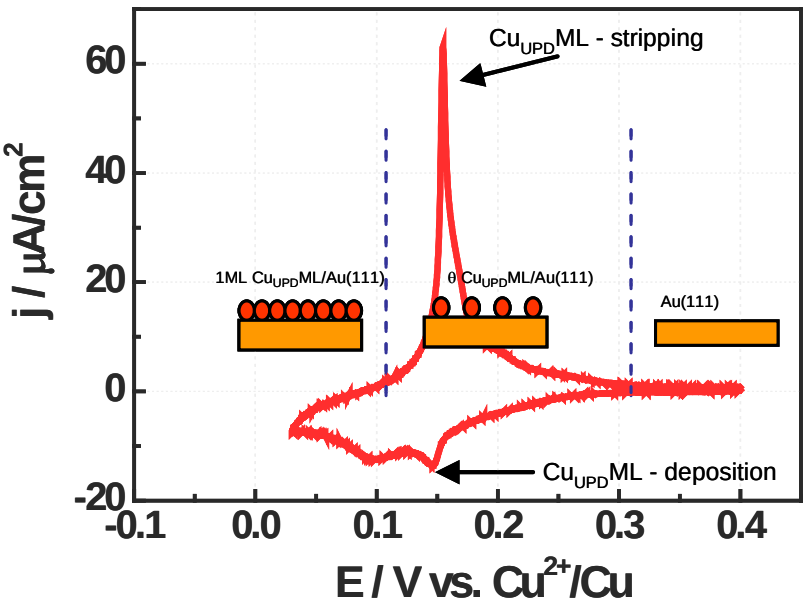

Figure 3-2. Cyclic voltammetry of Cu UPD on Au(111) in 10^{-3} M Cu^{2+} + 0.1 M $HClO_4$. solution with sweep rate 10 mV/s. The deposition and stripping peaks of Cu UPD ML are indicated [19].

The cyclic voltammetry is the principal technique to study UPD phenomenon and determine parameters such as potential, charge and coverage. Coverage of adatoms has proportional relation with stripping charge and varies with applied potential [20]. Thus,

by varying these parameters different type of surface can be achieved. The coverage and monolayer formation mostly depend on the attractive forces between the UPD metal and the substrate and interactions among the adatoms in the UPD layer. Furthermore, the effect of strain due to the lattice mismatch between the substrate and the UPD ML, the anion co-adsorption, as well as the double layer effects are also important for complete understanding of UPD [21].

The underpotential deposition technique can be used as initial method for further modification of metal-metal system.

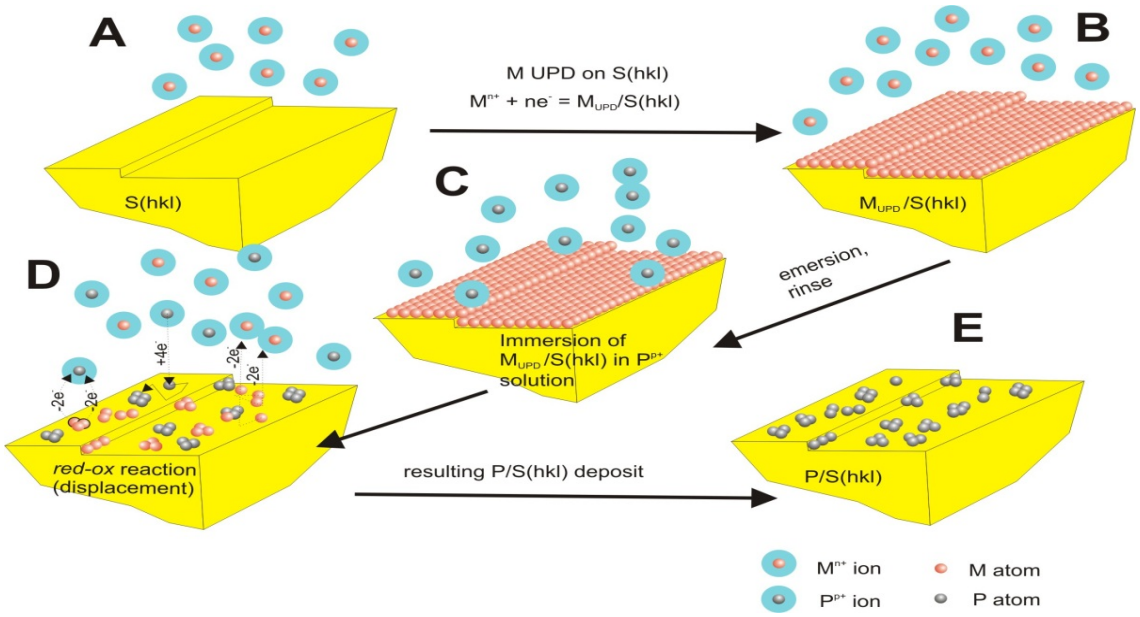

Figure 3-3. The basic steps of the deposition method. A-B: formation of *M* UPD ML on *S(h,k,l)*, B: $M_{UPD}/S(h,k,l)$ surface emersion from solution at certain potential ensuring the desired *M* UPD ML coverage of S(*h,k,l*) and/or number of UPD monolayers. C: transfer to P^{p+} containing solution at open circuit potential (OCP) conditions, D: *red-ox* or displacement reaction at OCP, E: final morphology of *P/S(h,k,l)* deposit [22]

Formed ML or ML's of metal *M* on substrate *S(h,k,l)* by UPD can serve as a sacrificial material for deposition of more noble metal *P* (Figure 3-3) [22]. The process is comprised of immersion of the crystal with ML of M_{UPD}/S(*h,k,l*) into the solution with P^{p+} ions, at

open circuit potential. The deposition of *P* occurs as an irreversible surface controlled red-ox reaction where the amount of deposited metal *P* is controlled by reaction stoichiometry, structure and coverage of the UPD ML/MLs (3-2) [5],

$$(b\cdot\theta\cdot q)\cdot M^{0}_{UPD}/S(h,k,l)+(b\cdot\theta\cdot q)\cdot\left(\frac{m}{p}\right)P^{p+}_{solv}\rightarrow(b\cdot\theta\cdot q)\cdot M^{m+}_{solv}+(b\cdot\theta\cdot q)\cdot\left(\frac{m}{p}\right)P^{0}_{s}/S(h,k,l)\ , \quad (3\text{-}2)$$

here, *m* and *p* are the oxidation states of UPD metal *M* and noble metal *P*. The factors *b*, θ, and *q* are introduced to accurately express the amount of deposited metal *P* in ML units with respect to atomic areal density of the substrate *S(h,k,l)* [5]. They represent the number of full UPD MLs, the UPD ML coverage, and the packing density of *M* atoms in complete UPD ML with respect to the substrate *S(h,k,l)*. The subscripts *s* and *solv* indicate the physical state of the metal (*solv* = solution phase and *s* = deposited). Since the UPD process is controlled by potential, coverage control to a fraction of a monolayer can be achieved [5]. Thus, the same accuracy for deposition of metal P via galvanic displacement of UPD metal M can be expected. This method can serve as a model for big improvements in the design of the catalyst monolayer, the preparation of sub-monolayers (SML) of noble metals with different coverage and morphology [19], and deposition of ultrathin films [19]. The electrochemical equilibrium potential of *P*electrode in contact with P^{p+} ions in the solution phase and the equilibrium potential of $M_{UPD}/S(h,k,l)$ at $\theta_{UPD}\rightarrow 0$ limit has positive difference. This serves as an electrochemical driving force for the surface limited redox replacement reaction (SLRR) defined as [23, 24]:

$$\Delta E_{red-ox}=\Delta E^{0}_{EMF}-\Delta E^{0}_{\theta\rightarrow 0}-\frac{RT}{F}\ln\frac{[a_{M^{n+}}]^{n}}{[a_{P^{p+}}]^{p}}>0\ , \quad (3\text{-}3)$$

here, ΔE^{0}_{EMS} ($\Delta E^{0}_{EMF} = E^{0}_{Pp+/P} - E^{0}_{Mn+/M}$) represents the electromotive force for the bulk *M* and *P* galvanic couple at standard conditions. The $\Delta E^{0}_{\theta \to 0}$ represents the equilibrium potential of $M_{UPD}/S(h,k,l)$ at $\theta_{UPD} \to 0$ limit at standard conditions ($a_{M}^{n+}=1$). Depending on combination of the $M_{UPD}/S(h,k,l)$ and P^{p+} ions and their oxidation states (for example Pt^{4+} *vs.* Pt^{2}) involved in the *red-ox* reaction, a different morphology and amount of *P* deposit can be formed (Figure 3-4) [19].

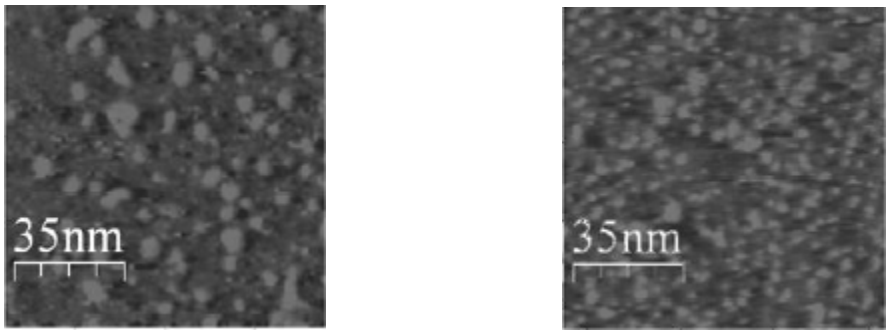

a) b)

Figure 3-4. STM morphology images for Pt deposition (a) via SLRR of Pb_{UPD}/Au (111) and (b) via SLRR of Cu_{UPD}/Au (111), in 10^{-3} M $\{PtCl_6\}^{2-}$ + 0.1 M H_2SO_4 electrolyte.

CHAPTER 4: EXPERIMENTAL PROCEDURE

The two Platinum and two Palladium single crystals (Monocrystal Co.) with (111) and (100) plane orientation were used as a working electrodes (WE). The diameters of single crystals are 10 mm with thicknesses of 3 mm. The surface preparation included mechanical polishing and propane flame annealing. First, the crystals were mechanically polished using 1 and 0.25 μm diamond suspensions until visible clean and smooth surface were obtained. After mechanical polishing and flame annealing the crystals were sonificated in distillated water and thoroughly rinsed with 18.2 MΩ ultrapure water (Milipore Direct Q-UV with Barnstead A1007 pre-distillation unit). Following that, single crystals were held in the propane flame for 15 minutes to create cleaner and smoother surfaces (Figure 4-1).

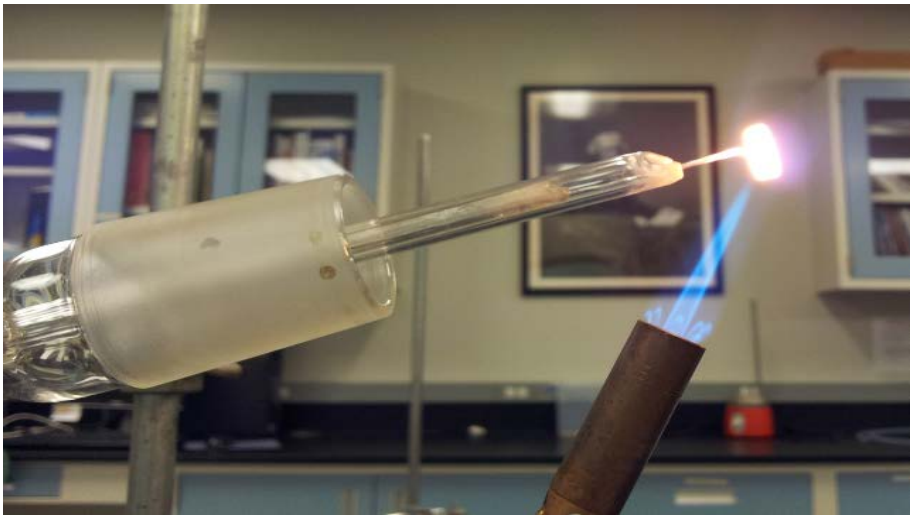

Figure 4-1. Propane flame annealing of the single crystal on the temperatures giving glowing red-hot look of the crystal.

The cooling of Pt electrodes was done with argon gas containing 4% of hydrogen (mild reductive) in oxygen free environment (Figure 4-2).

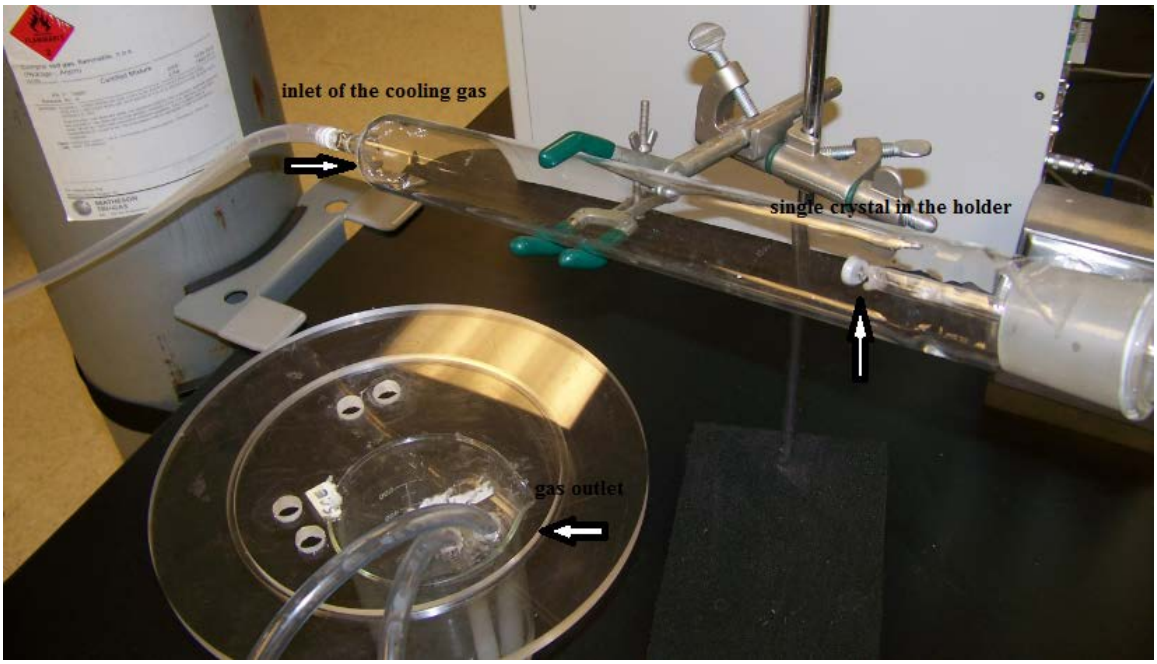

Figure 4-2. The single crystal cooling setup.

The hose coming from the tube with the crystal was immersed in the water at the end to prevent any inlet of the air to the tube. The Pd crystals were cooled down in the same way but using pure argon gas to prevent possible hydride formation (in the case of the hydrogen containing gas). After crystals are cooled down for several minutes they were transferred into the beaker with 18.2 MΩ ultrapure water prior to further uses.

Several cyclic voltammetry experiments were done with each crystal to confirm cleanliness and obtain characteristic *i-V* graph for specific material and surface plane orientation. After annealing and cooling, the single crystal under study was quickly transferred by protection of droplet of water to electrochemical cell with 0.05 M sulfuric acid electrolyte. The electrolyte was dearated for two hours with high purity nitrogen gas to remove oxygen from environment. The working electrode was set as hanging meniscus configuration in the contact with electrolyte (Figure 4-3).

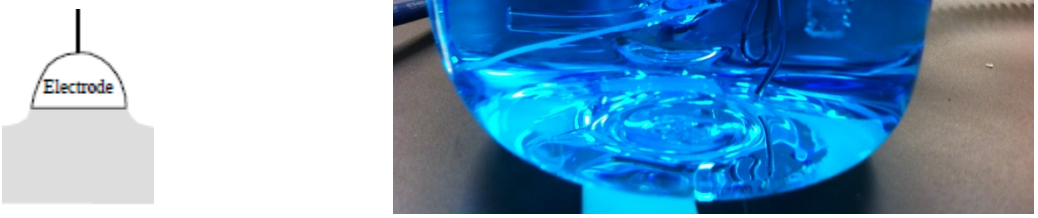

Figure 4-3. The hanging meniscus configuration in the EC cell for cyclic voltammetry characterization.

The Pt wire was used as a counter electrode (CE) in all cyclic voltammetry experiments and was annealed prior to each measurement for cleaning purposes. As reference electrode (RE), the saturated calomel electrode (SCE) was used with salt bridge containing 0.05 M sulfuric acid solution. The electrochemical measurements were carried out using Autolab PGSTAT12 potentiostat as well as BASI Epsilon EC potentiostat. These potentiostats were used in all electrochemical measurements including copper UPD and open circuit potential measurement (OCP). During the CV scans, nitrogen purging was continued inside the cell above the electrolyte.

The UPD and SLRR processes took place in the similar setup (Figure 4-4). The solutions were prepared using ultrapure chemicals (99.999%, Alfa Aesar, J.T.Baker) and 18.2 MΩ ultra-pure water.

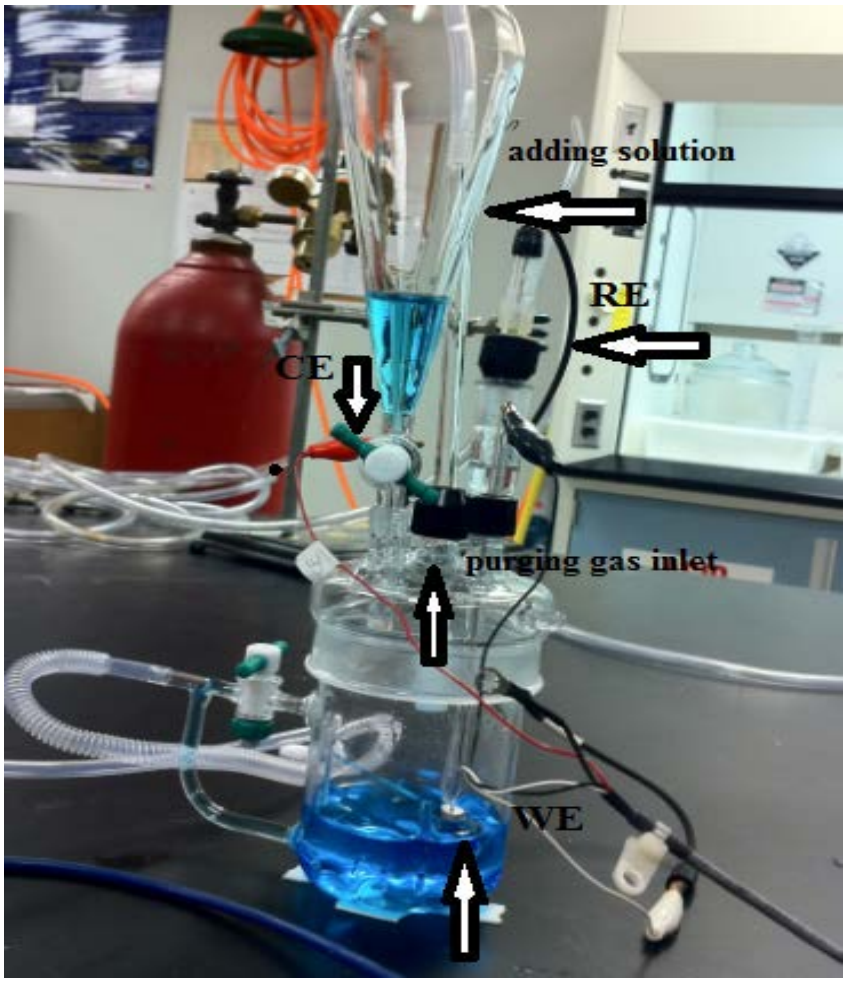

Figure 4-4. The electrochemical cell for the UPD and SLRR experiments.

The glassware and Teflon parts of the cell were cleaned in piranha solution (1:3 H_2O_2, H_2SO_4) prior to the experiments. The Cu UPD was carried out in electrolyte which was dearated with high-purity nitrogen gas for two hours to eliminate oxygen content because of the susceptibility of Cu(UPD) layer to oxygen reduction and its own dissolution. The experimental routine for Pt deposition by SLRR of Cu(UPD)/Pd(100) and Cu(UPD)/Pd(111) took following steps:

Step 1: Prior to Cu UPD layer formation the cyclic voltammetry with hanging meniscus configuration, the surface characterization was performed showing the characteristic peaks for Cu UPD on Pd(hkl)

Step 2: Formation of Cu(UPD)/Pd(hkl) at a certain potential (~200 mV vs. SCE) in 0.35 M $CuSO_4$ + 0.05 M H_2SO_4 for 600 seconds.

Step 3: After 25 seconds from start of open circuit potential measurements, the addition of 10 ml of solution containing 0.00255 M $\{PtCl_6\}^{2-}$+ 0.05 M H_2SO_4 began. Solution was added to the electrolyte drop by drop for 5-7 minutes (until all solution is added). This step was also carried out with another design of adding solution following the common first two steps. The second design of solution contained 0.2086 M citrate ions + 0.00255 M $\{PtCl_6\}^{2-}$ + 0.05 M H_2SO_4. The redox replacement was monitored at OCP for 1800 seconds.

Step 4: After OCP, crystal is taken from the cell and rinsed with 18.2 MΩ water or, in the case of citrate ions, crystal is rinsed with the ultra-pure water then kept in the hot sulfuric acid for 15 seconds and rinsed again.

The crystal was kept in ultra-pure water prior to the transfer to the electrochemical cell within SNIFTIRS unit.

The SNIFTIRS data were measured using a NICOLET 6700 FTIR apparatus equipped with a MCT-A detector cooled with liquid nitrogen. The compartments were purged using compressed air with inlet pressure at 60 psi from a Parker Balston Purge Gas Generator with 9 $Lmin^{-1}$ flow rate, which was free of CO_2 and H_2O. The electrode potential was controlled by BAS CV-27potentiostat. The cell with a hemispherical ZnSe

window was employed in these studies. The separate, sample compartment was specially designed for this type of experiments. Detector was moved from original FTIR spectrometer compartment and mounted in the sample compartment. Then, the system of the parabolic (f=6") and flat mirrors was constructed to direct the collimated infrared beam from the spectrometer to the working electrode (Figure 4-5).

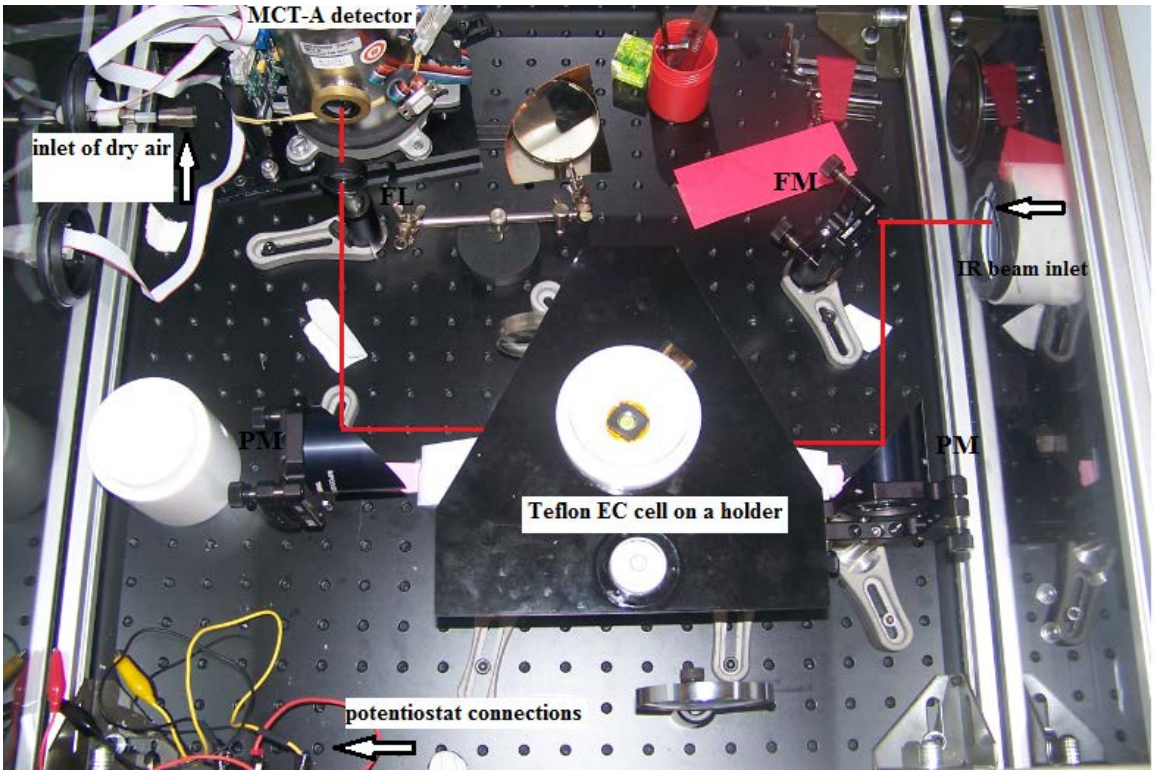

Figure 4-5. The sample compartment with the electrochemical cell and mirrors setup. FM - flat mirror; PM - parabolic mirror; FL - focusing lens.

The angle of incidence θ was calculated to be just above (~2 $^{\circ}$) the critical angle θ_c of water/ATR. The calculations are presented in the Figure (4-6).

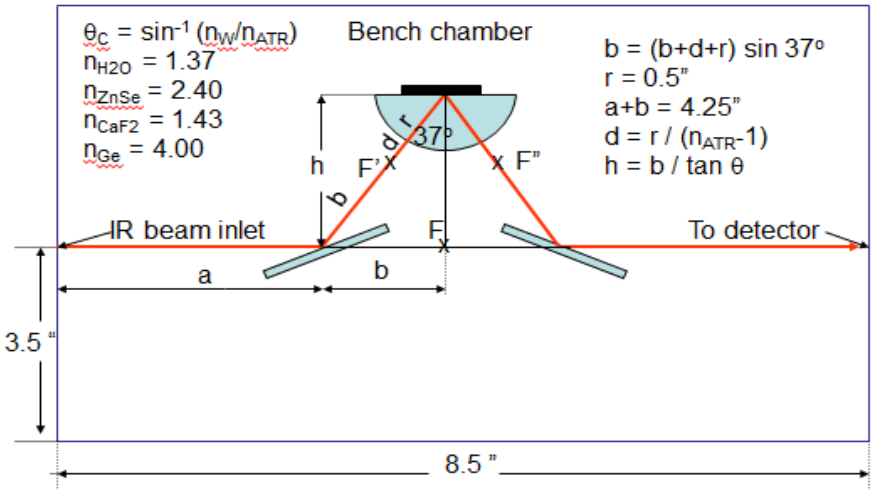

Figure 4-6. The schematics of beam path and calculation of the setup parameters.

here n_w and n_{ATR} are refraction indices for the water (the major component of solution) and ZnSe optical material. To obtain ATR the refractive index of optical material has to be higher than one of the electrolyte which has direct effect on calculation of critical angle θ_c. For our setup the θ_c is calculated for the water-ZnSe interface i.e. arcsine(1.73/2.4) gives the 35 ° for critical angle. The angle of incidence is then adjusted to be around 37 ° (Figure 4-6 and 4-7).

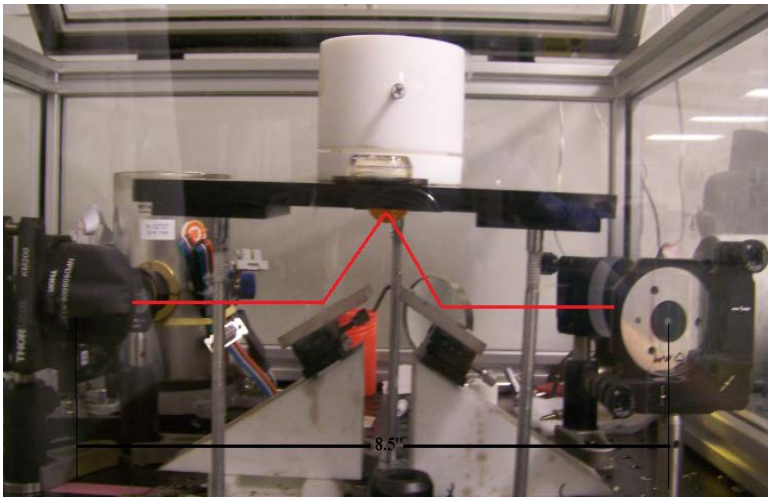

Figure 4-7. The path of the beam from the mirrors to the optical window in EC cell.

Some of the SNIFTIRS parameters for different setups i.e. optical windows are given in Table 4-1.

ZnSe	CaF2	Ge	Si
$\theta_C \sim 35°$ $\theta = 37°$ d = 0.35” b = 1.29” a = 2.96” h = 1.72”	$\theta_C \sim 73°$ $\theta = 75°$ d = 1.25” b = 49.6” (Impossible)	$\theta_C \sim 20°$ $\theta = 22°$ d = 0.17” b = 0.40” a = 3.85” h = 0.99”	$\theta_C \sim 26°$ $\theta = 26°$ d = 0.21” b = 0.55” a = 3.69” h = 1.13”

Table 4-1. The calculation of parameters for different optical window material.

The spectroelectrochemical cell (SEC) (see Figure 4.7), was custom-made of Teflon and connected to the optical window (ZnSe) via a Teflon tape. The working electrode (WE) was inserted into a glass tube, which was used to push the electrode against the optical window. The WE is then placed in SEC cell filled with electrolyte (0.25 M sulfuric acid or 0.1 M perchloric acid) equipped with the reference electrode (MSE or SCE) and counter electrode (Pt wire). Firstly, sample potential was applied E_1 = -0.500 V (MSE). Following, the WE is pushed against the optical window and appreciable increase of interferogram peak-to-peak signal is achieved on specific position of the crystal onto ZnSe window (Figure 4-8).

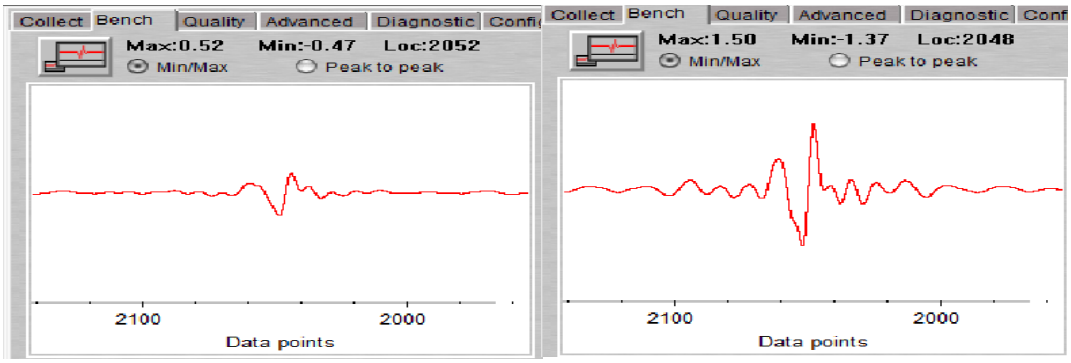

Figure 4-8. Peak-to-peak signal before and after placing the crystal on the ZnSe window.

This is used as a criterion of a good initial position of the electrode in the cell. Then, the sample compartment is closed and dry compressed air is purged for two hours to eliminate water and carbon-dioxide from the environment. During this time the potential was kept on -0.5 V (vs. MSE). The solution is purged at the same time with argon to remove CO from bulk solution. This way only remained CO was CO ML adsorbed on the electrode surface during the IR experiment. After two hours the potential was stepped by 0.100 V in positive direction and at each potential interferogram was collected with 20 seconds of delay between setting (potential switch) and measurements (interferogram collection) to allow the interface to reach equilibrium. The final sample interferogram was collected at potential of 0.100 V. The background interferogram was collected at 0.500 V where all adsorbed CO is expected to be oxidized. In the case when perchloric acid solution was used as an electrolyte reference electrode was SCE and corresponding potentials for initial adsorption of CO, final potential and background potential were -0.1 V, 0.5 V and 0.9 V, respectively. Each collection was done at 8 cm^{-1} resolution with 128 scans. The interferograms are further processed by OMNIC software to obtain characteristic spectra.

CHAPTER 5: RESULTS AND DISCUSSION

5.1. Electrochemical Surface Characterization

The single crystals surface preparation procedure developed by Clavilier [25] serves as a qualitative and easy method for achieving conditions to obtain reliable electrochemical data. These conditions being intrinsic to a high quality surfaces in terms of cleanliness and orientation gives specific features to cyclic voltammetry in the water based electrolytes. Hence, the voltammetric profiles on the surfaces with different atoms and plane orientation serve as a fingerprint of the structural conditions [27]. The different adsorption processes taking place at the platinum/electrolyte surfaces, in 0.05 M sulfuric acid solution, with different plane orientation are present in the Figure 5-1-1 with corresponding voltammograms.

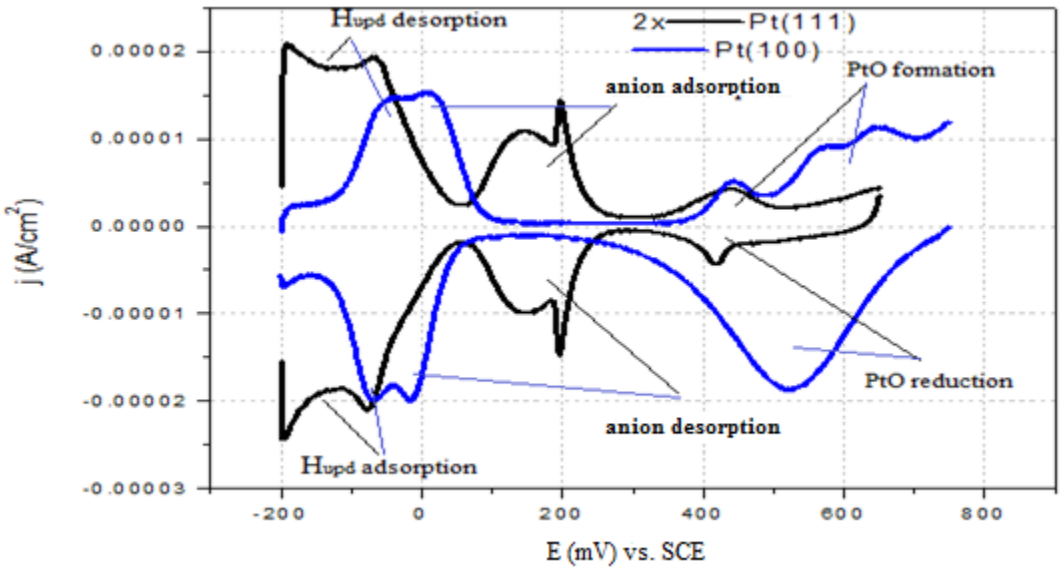

Figure 5-1-1. A cyclic-voltammetry profile for Pt(111) and Pt(100) obtained in 0.05 M aq. H_2SO_4 recorded at a scan rate of $\nu = 20$ mV s^{-1} (preparation procedure explained in the chapter 4).

The observation of characteristic CV features for Pt(111) corresponds to hydrogen adsorption-desorption region, i.e., -0.2 V < E_{SCE} < 0.05 V, anion ((bi)sulphate) adsorption-desorption in region 0.05 V< E_{SCE} < 0.25 V and Pt oxidation-reduction region, 0.25 V < E_{SCE} < 0.65 V. Obtained graphs are consistent with the literature data for these surfaces [26,27,28,29]. The Pt(100) exhibits different potential regions for same processes: H_{UPD} which is immediately followed by anion adsorption in the region of -0.15 < E_{SCE} < 0.05 and Pt oxidation at higher potentials [27,30,31]. Also, the corresponding cyclic voltammetry curves are obtained for palladium/electrolyte surfaces with different surface orientation (Figure 5-1-2).

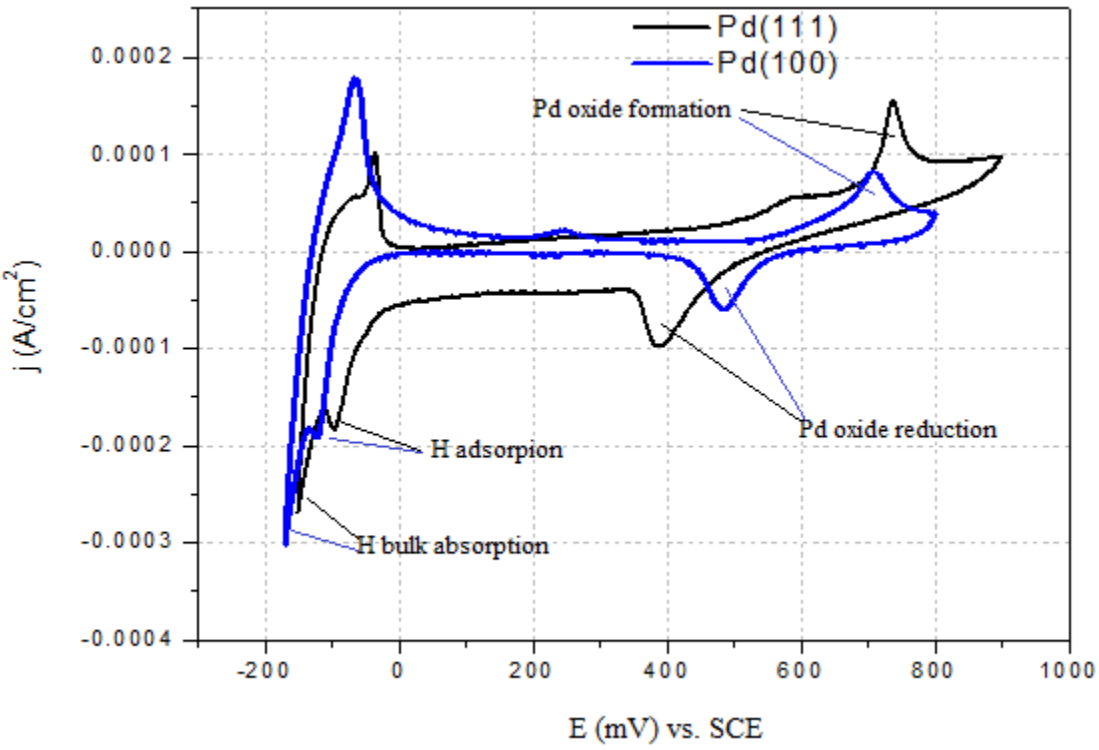

Figure 5-1-2. A cyclic-voltammetry profile for Pd(111) and Pd(100) obtained in 0.05 M aq. H_2SO_4 recorded at a scan rate of $\nu = 20$ mV s^{-1} (preparation procedure explained in the chapter 4).

The potential of Pd(111) electrode was initially scanned from 0.9 V vs. SCE in the negative direction. The sharp peak at the 0.39 V is associated with the reduction of Pd oxide. By further increase of cathodic current CV features are observed at potentials -0.09 V which correspond to hydrogen adsorption, followed by the peak for hydrogen absorption into the bulk of the crystal at potential of *ca.*-0.12 V. In the positive scan, the corresponding reverse reactions of hydrogen bulk desorption and surface desorption (-0.15 V < E_{SCE} < - 0.02 V potential region), as well as Pd oxide formation at 0.75 V can be seen [32,33]. The small peak at 0.59 V is associated with anion (bisulphate) adsorption. The voltammetric curve for Pd(100) showed similar behavior with difference in the potential regions of hydrogen adsorption (-0.12 V) and bulk absorption with onset potential *ca*. -0.150 V. The Pd oxidation and reduction were observed at 0.710 V and 0.450 V, respectively. The small peak at ca.0.22 V could be explained by order/disorder phase transition in the adsorbed sulfate adlayer on Pd(100) [32,33,34].

5.2. Cu UPD on Pd(hkl)

The underpotential electrodeposition (UPD) of copper atoms on Pd(111) or Pd(100) surfaces was employed and each surface was subjected to characterization by cyclic voltammograms. The electrolyte solution for this process was 0.35 M $CuSO_4$ + 0.05 M H_2SO_4. The potential was scanned in the negative direction at 5 mV/s and stopped at potential before the onset of copper bulk deposition. At that point the scan direction was reversed and scanning was stopped at a potential before Pd oxidation. The system Cu/Pd(hkl) has the advantage that desorption of Cu atoms due to stripping occurs before the onset of Pd oxide formation [35]. Typical voltammograms on Pd(111) and Pd(100) are shown in Figure 5-2-1 and 5-2-2, respectively. During the cathodic sweep,

sharp deposition peak (1) for Cu(UPD)/Pd(111) appeared at 0.258 V. The stripping peak (2) occurred at 0.284 V. Deposition and stripping peaks show reversible characteristics and peak shapes were consistent after repetitive cycles. The charge recorded to strip a Cu(UPD) ML on Pd(111) was ~273 μCcm^{-2}. The result for stripping charge is in fairly agreement with results from earlier studies (460 μCcm^{-2} [33]). The discrepancy can be explained due high concentration of anions in solution used in this work compared to more diluted solution in previous studies. Simultaneous anion adsorption causes that measured Cu UPD charge is lower.

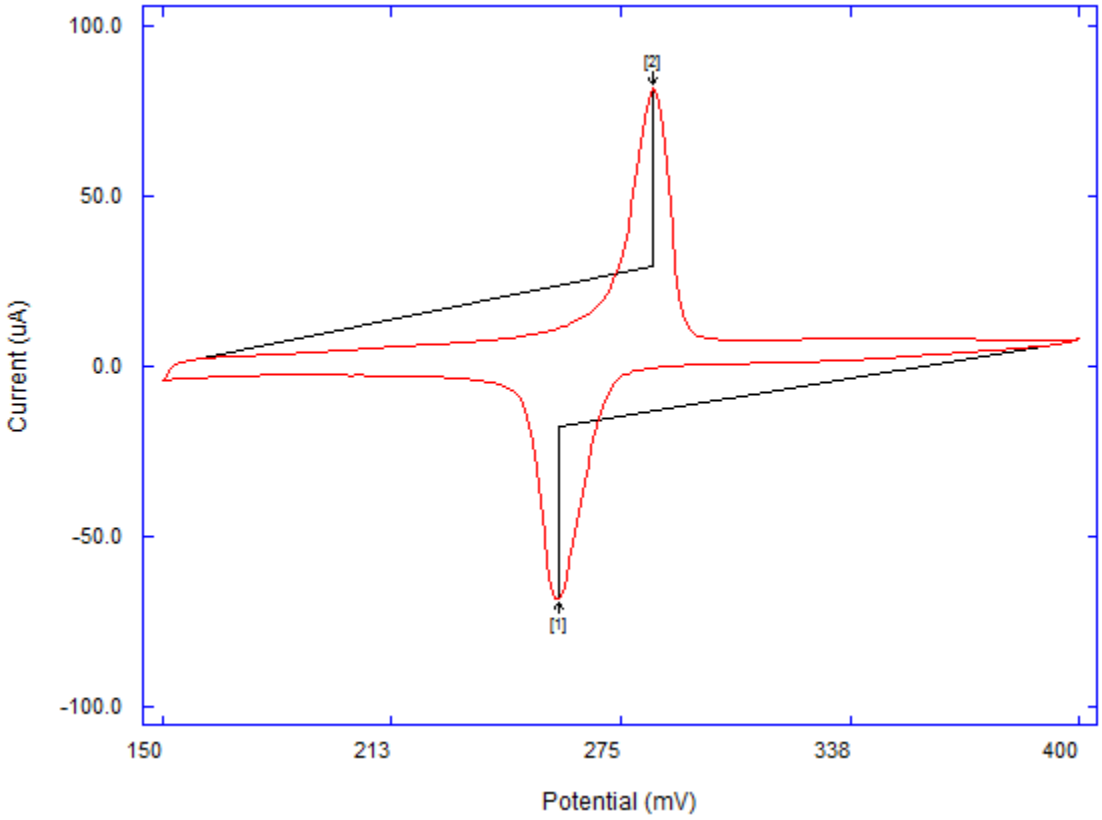

Figure 5-2-1. Cyclic voltammetry of Cu(UPD)/Pd(111) from a 0.35 M $CuSO_4$ + 0.05 M H_2SO_4 solution. Sweep rate 5 mV/s with SCE as reference electrode.

The adequate pretreatment of the single crystals is also confirmed for Pd(100) system by Cu UPD. Figure 5-2-2 shows the characteristic voltammogram for Cu adsorption on the Pd(100) surface.

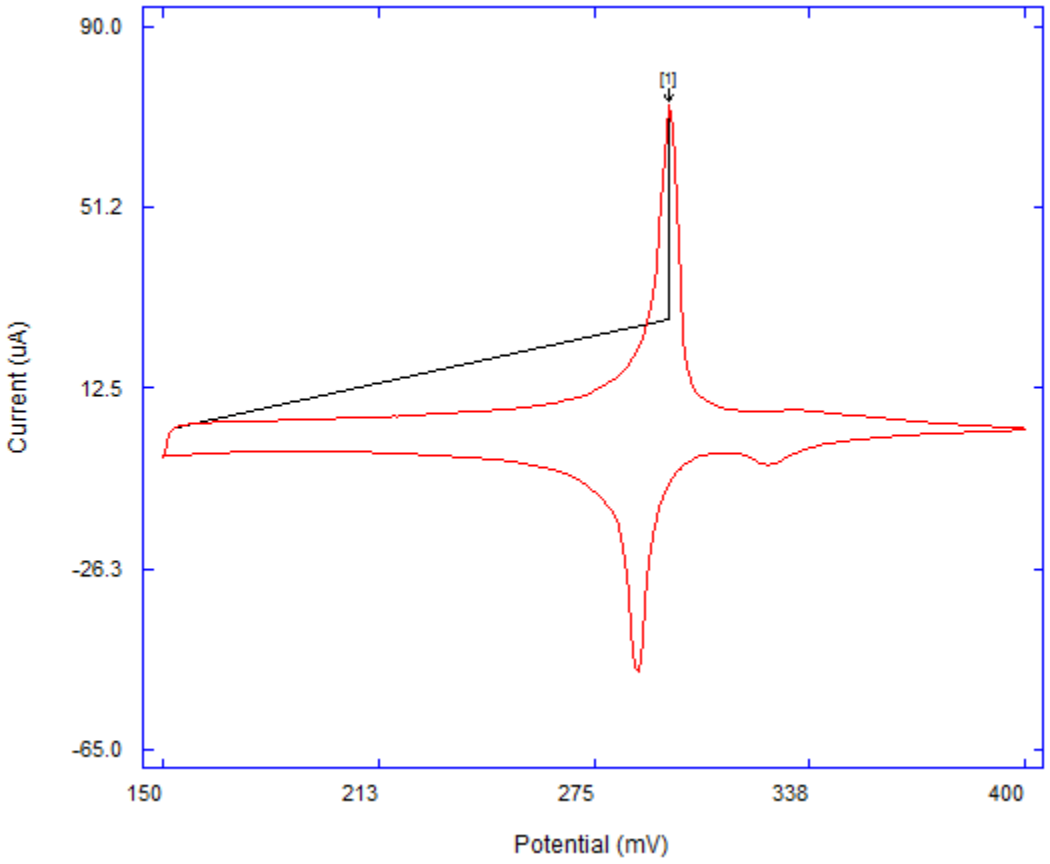

Figure 5-2-2. Cyclic voltammetry of Cu(UPD)/Pd(100) from a 0.35 M $CuSO_4$ + 0.05 M H_2SO_4 solution. Sweep rate 5 mV/s with SCE as reference electrode.

The characteristic deposition sharp peak occurred at 0.287 V. The stripping peak (1) with associated stripping charge of ~ 271 μCcm^{-2}, appeared at 0.297 V at the anodic sweep direction which is in agreement with earlier studies [33,35]. The small peaks at ca. 0.350 V occurred due to Cu UPD on surface steps.

5.3. Pt deposition via SLRR

The typical cyclic voltammograms for Cu(UPD)/Pd(hkl) systems are shown in Figures 5-2-1 and 5-2-2. The same quality of the voltammetry in each experiment has been obtained routinely before the potential hold step at 0.2 V underpotential to form full Cu(UPD)/Pd(hkl). After Cu ML is formed the solution containing $\{PtCl_6\}^{2-}$ is added and change in the electrode potential during redox replacement of Cu atoms by Pt ions: Cu(UPD)/Pd(111) + $\{PtCl4\}^{2-}$ = Pt_{dep}/Pd(111) + Cu^{2+} + $4Cl^-$ is monitored at open circuit potential.

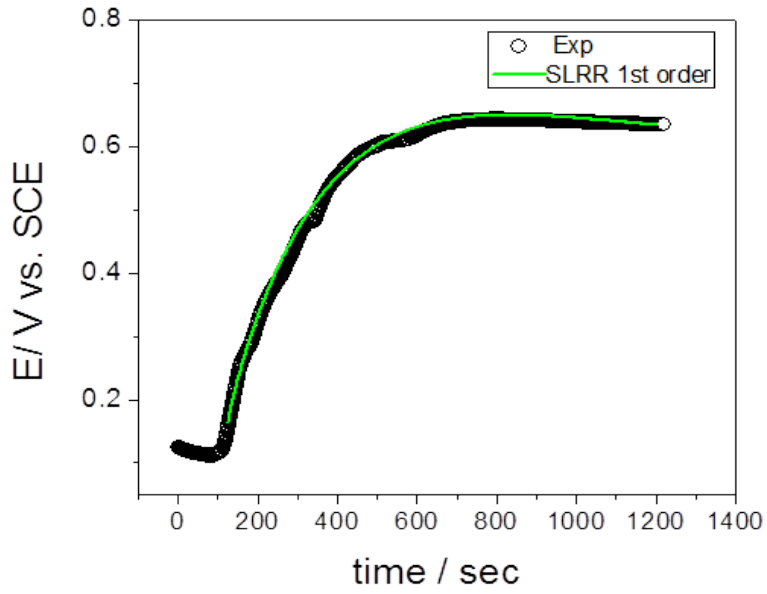

Figure 5-3-1. OCP transient during galvanic displacement for 0.00255 M $\{PtCl_6\}^{2-}$ + 0.05 M H_2SO_4 solution. Line indicates model of SLRR of the first order [19].

The characteristic OCP transient curves are obtained for both adding solutions: Figure 5-3-1 for solution containing 0.00255 M $\{PtCl_6\}^{2-}$ + 0.05 M H_2SO_4 (design I) and Figure 5-3-2 for solution containing 0.00255 M $\{PtCl_6\}^{2-}$ + 0.05 M H_2SO_4+ 0.2086 M citrate ions (Cit^{3-}) (design II).

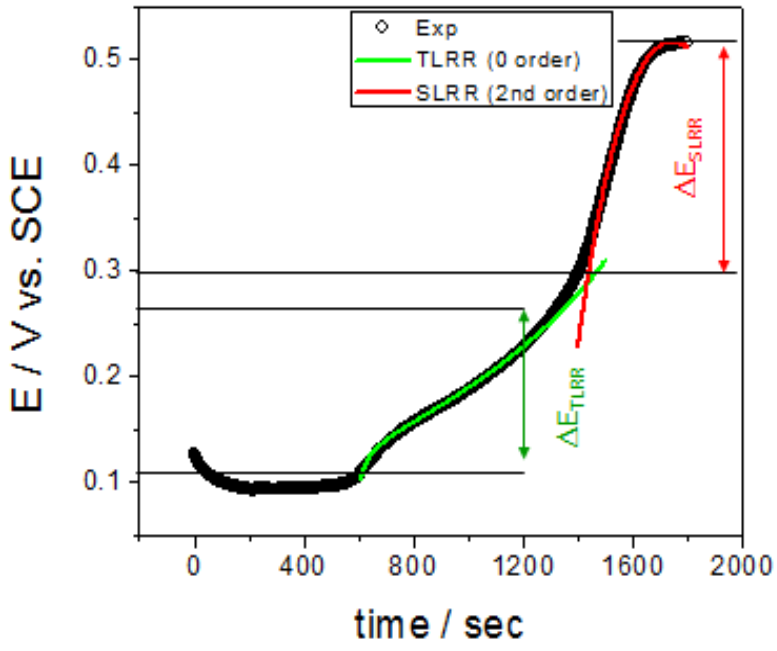

Figure 5-3-2. OCP transient during galvanic displacement for 0.00255 M $\{PtCl_6\}^{2-}$ + 0.05 M H_2SO_4 solution + + 0.2086 M citrate ions (Cit^{3-}). Green line indicates model of the SLRR of the zeroth order. Red line indicates model of the SLRR of the second order.

The reaction kinetics for solution I is best described by 1st order surface limited red-ox replacement reaction (SLRR) as expected from stoichiometry of the galvanic displacement reaction (equation 3-2) with calculated constant of <k"> = $0.0021\pm8.4\times10^{-6}$ s^{-1}[19]. The OCP transient curve for adding solution II showed different features with two distinct parts. The first transient region (green color) after potential starts increasing can be explained by transport limited red-ox replacement reaction (TLRR) according to equations [19]:

$$E = E_{\theta\to 0} - \frac{RT}{mF}\cdot \ln\left\{\begin{array}{l}\dfrac{(1-k_0 t)}{k_0 t} + \\ f\cdot(1-k_0 t) + g\cdot(1-k_0 t)^{3/2}\end{array}\right\} \quad (5\text{-}3\text{-}1)$$

,

$$k_0 = \left(\frac{m}{p}\right) \cdot \frac{D_{P^{p+}} \cdot C^{\infty}_{P^{p+}}}{\delta} \cdot \Gamma_{UPD} \quad , \qquad (5\text{-}3\text{-}2)$$

which follows zero order of reaction kinetics. The TLRR is limiting situation of SLRR when the transport of the noble metals (Pt) ions from the bulk solution to the electrode is the limiting step. The rate then equals to the flux of the arriving P^{p+} ions to the electrode surface, $F_p = \cdot \frac{D_{P^{p+}} \cdot C^{\infty}_{P^{p+}}}{\delta}$ where $D_{P^{p+}}$ and δ are the diffusion coefficient of P^{p+} ions and the thickness of the diffusion layer, respectively. The $C^{\infty}_{P^{p+}}$ is the concentration of the P^{p+} ions in the bulk of solution and Γ_{UPD} is the full Cu UPD ML. The obtained value for k_0 is $(9 \pm 2) \times 10^{-4} s^{-1}$. For the second transient region (red color), there is no transport limitation for P^{p+} ions and the reaction follows the second order reaction kinetics with calculated rate constant of <K> = (1.25±0.17) x 10^{-3} s^{-1}. To explain the citrate effect on this transport limiting behavior of the system the several linear sweep voltammetries (LSV) were obtained.

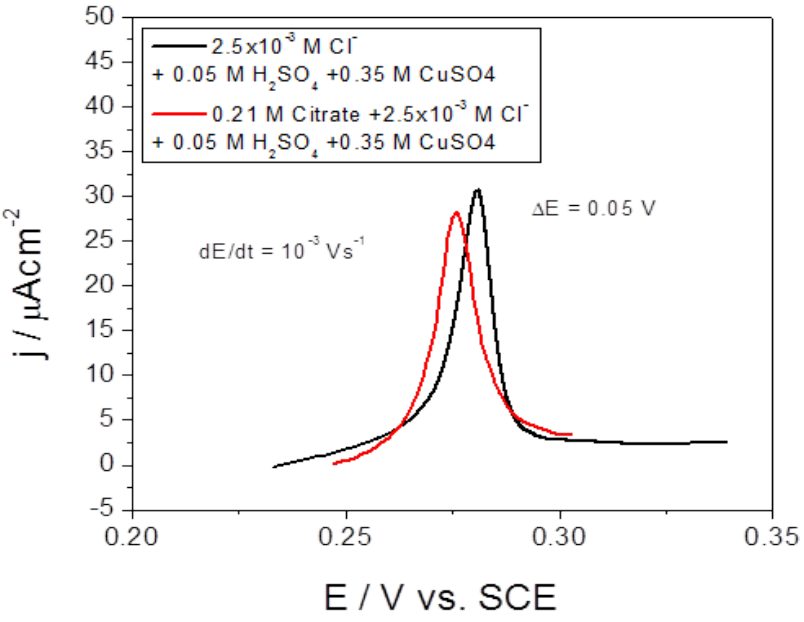

Figure 5-3-3. The LSV features during the UPD stripping.

Firstly, the Cu UPD is formed in the electrolyte containing chloride ions (2.5 mMCl- + 0.35 $CuSO_4$+ 0.05 H_2SO_4) and stripping sweep potentials are applied in the positive direction. Secondly, the same procedure is carried out for the second solution containing citrate, added upon UPD formation, and chloride ions (2.5 mM Cl^- + 0.35 $CuSO_4$ + 0.05 H_2SO_4 + 0.21 M Cit^{3-}). The corresponding LSV curves are present in Figure 5-3-3. The difference in stripping potential of 5mV is found negligible leading to conclusion that there is no formation of $Cu/\{CuCit^{(2+3x)}\}$ complex and no citrate effect on stripping potential.

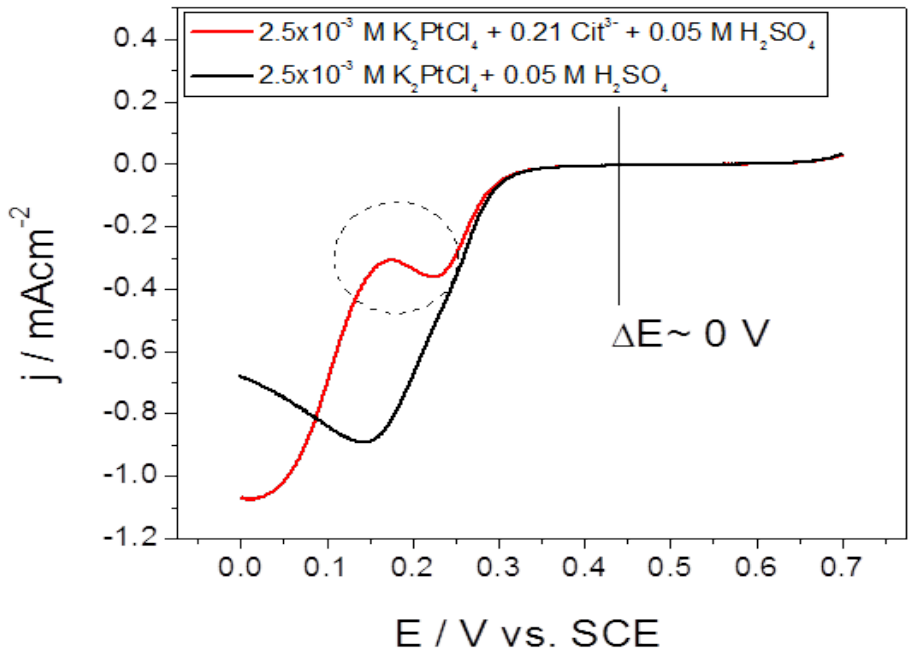

Figure 5-3-4. LSV features during the deposition.

Then another set of the LSV experiments is carried out. This time solutions contained $\{PtCl_6\}^{2-}$ i.e. solution I contained 0.00255 M $\{PtCl_6\}^{2-}$ + 0.05 M H_2SO_4 and solution II contained 0.00255 M $\{PtCl_6\}^{2-}$ + 0.05 M H_2SO_4 + 0.2086 M citrate ions. This time sweep was in negative direction and deposition of the Pt occurred. The observed data did not show any difference in the Pt reversible potential (onset of deposition) between citrate containing solution and solution without citrate. That led to conclusion that there is no formation of $Pt/\{PtCit_X\}^{(4+3X)}$ complex. However, the inhibition of Pt deposition kinetics by Cit^{3-} ions is observed in potential range between 0.15 V and 0.25 V which is in correspondence with the TLRR region of the OCP transient data. Excluding formation of the complexes with the ions in solution, the transport limiting behavior could be explained by citrate inhibition of the transport of the Pt ions by adsorbing on the surface

(TLRR part). After this region the citrate modifies transfer of the charge to Pt ions (SLRR 2nd order).

The morphology of Pt modified Pd(111) single crystal, with and without citrate ions in the solution was investigated by scanning tunneling microscopy (STM). The images (Figure 5-3-5 and 5-3-6) clearly showed difference in the morphology of deposits.

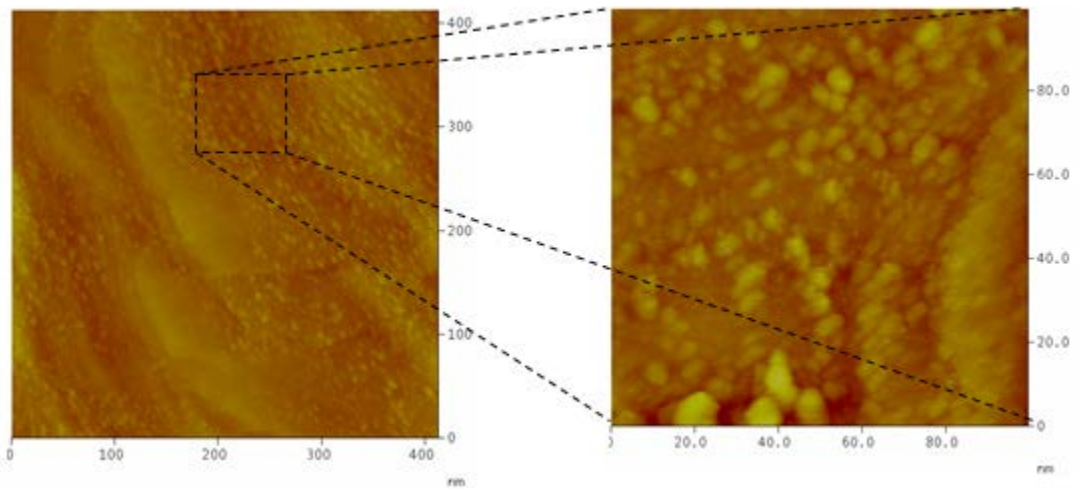

Figure 5-3-5. STM image of Pt modified Pd(111) surface via SLRR in 0.05 M H_2SO_4 +0.35 M $CuSO_4$ + 0.00255 M K_2PtCl_4.Image sizes: 400x400 nm and 100x100nm.

The STM image of the surface modified from solution electrolyte without citrate ion showed non-uniform deposits (Figure 5-3-5). Morphology appears as individual separate Pt nanoclusters, average size ~5.3 nm. There are also populations with clusters having average size of 8 nm. The average height of majority of the clusters is two (or more than two) monolayers (> 0.8 nm). The surface modified with the citrate ions in solution has a different morphology of deposits (Figure 5-3-6).

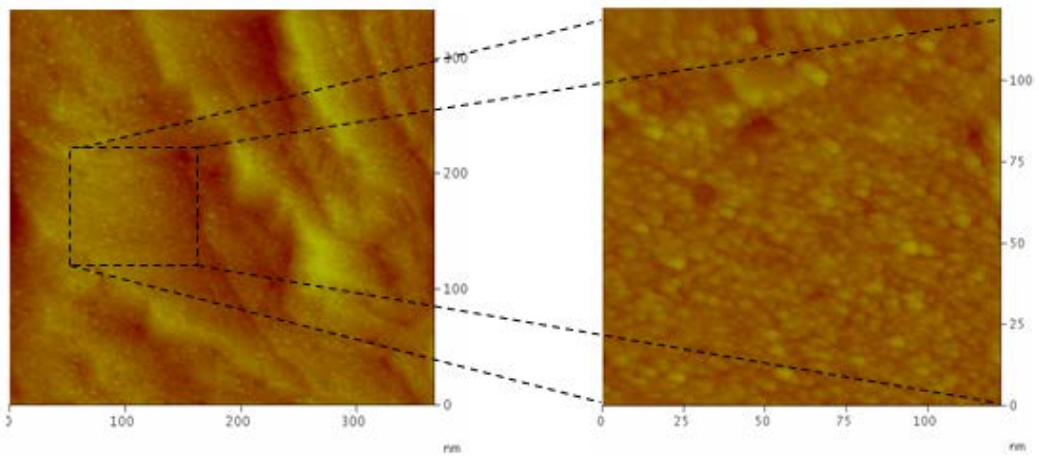

Figure 5-3-6. STM image of Pt modified Pd(111) surface via SLRR in 0.05 M H_2SO_4 +0.35 M $CuSO_4$ + 0.00255 M K_2PtCl_4 + 0.21 Cit^{3-}. Image sizes: 400x400 nm and 125x125 nm

The deposit with citrate ions showed mostly very uniform coverage. Morphology appears as merged nanoclusters into a full monolayer, average sizes ~3 nm, most of the clusters are monoatomic height (0.43 nm) i.e., a true monolayer configuration.

The change in electrochemical behavior of the Pt monolayer modified Pd single crystals indifferent solutions is studied by obtaining several cyclic voltammetry on the surfaces. The corresponding CV curve (Figure 5-3-7) presents the voltammetry for monolayer of Pt on Pd(111). The characteristic spike for Pd oxide formation for clean Pd(111) single crystal at 0.75 V vanishes as expected. The Pt monolayer is formed on these surfaces which blocks the oxide formation of Pd(111) [33]. Instead, the characteristic features of Pt like oxide formation can be seen at higher potentials (> 0.75 V) with appropriate shape for different adding solution. Accordingly, the Pd(111) oxide reduction (at 0.39 V) is altered and for modified surfaces Pt oxide reduction features are obtained for the systems with citrate and without citrate in electrolyte solution. Furthermore, the observable features of anion adsorption for Pt_{ML}/Pd(111) with citrate

(at 0.32 V) and Pt_{ML}/Pd(111) without citrate (at 0.42 V) confirms the surface modification and different electrochemical behavior due to morphological change induced by citrate presence.

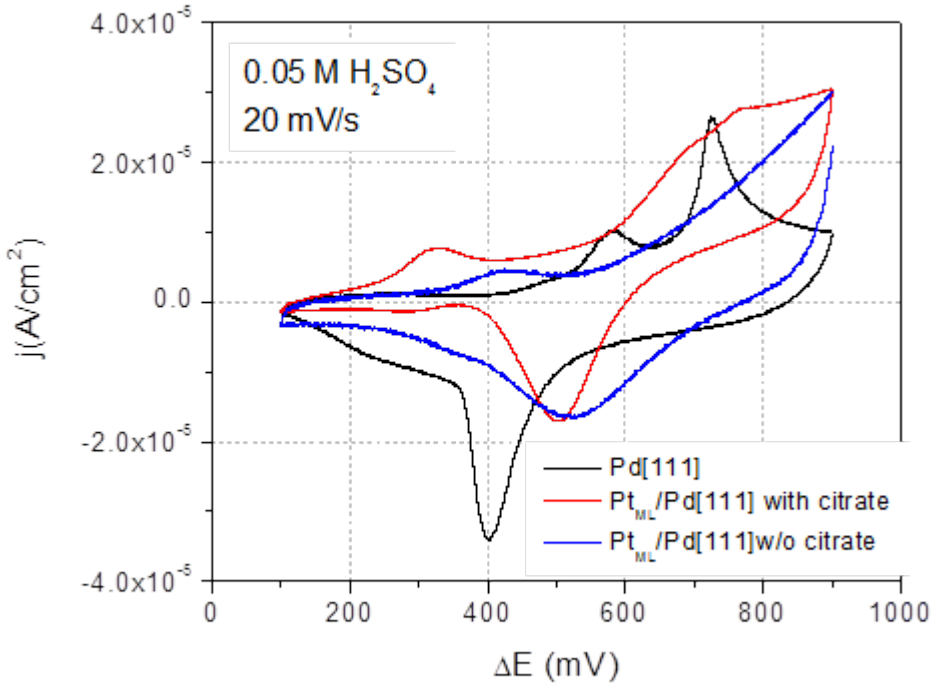

Figure 5-3-7. CV features for Pt modified Pd(111) surface from different electrolyte solution design compared with clean Pd(111) surface (short region sweep) in 0.05 M H_2SO_4.

The similar alteration of electrochemical behavior is obtained for the Pt modified Pd(100) surface (Figure 5-3-8). The Pd oxide formation and reduction peaks (0.71 V and 0.45 V respectively) disappeared at the modified surfaces with formation of the Pt like oxide features in positive scan and its reduction in negative scan. The anion adsorption features for modified surfaces verifies the Pt_{ML} formation.

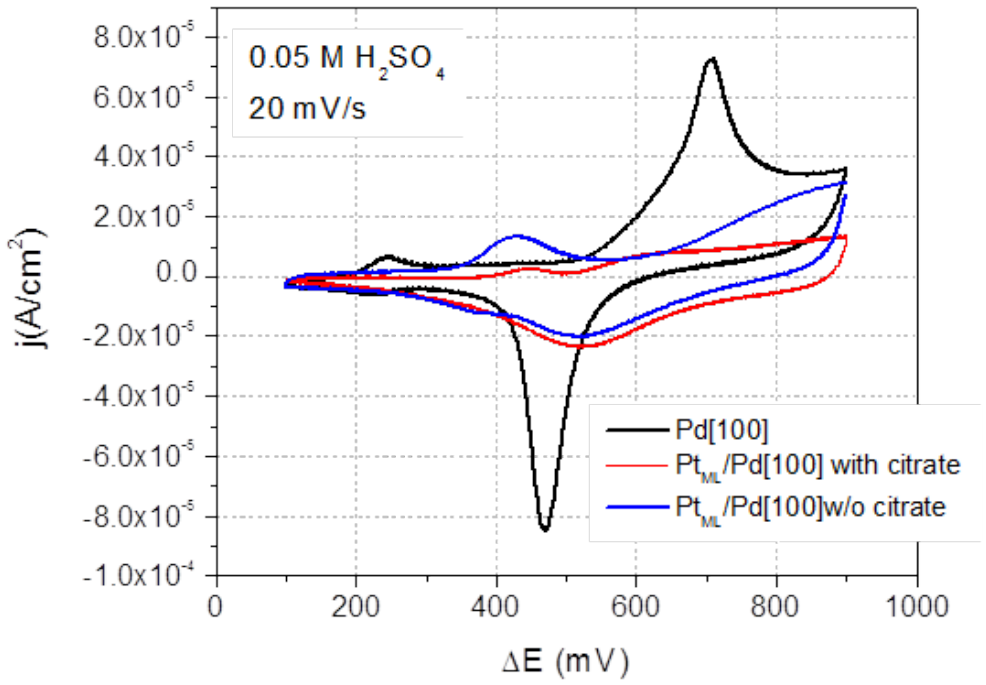

Figure 5-3-8. CV features for Pt modified Pd(100) surface from different electrolyte solution design compared with clean Pd(100) surface (short region sweep) in 0.05 M H_2SO_4.

5.4. SNIFTIRS results

Spectroscopic studies are performed on the Pt and Pd single crystals with (111) and (100) plane orientation, as well as on Pt_{ML}/Pd(111) and Pt_{ML}/Pd(100) surfaces synthetized Cu (UPD) of SLRR via with and without citrate presence. Furthermore, the cyclic voltammograms of CO oxidation are obtained on corresponding surfaces.

5.4.1. The (111) Plane orientation

Pt(111)

SNIFTIRS spectra of adsorbed CO on Pt(111) in 0.1 Mperchloric acid are shown in the Figure 5-4-1-1. The CO was adsorbed at -0.1 V (vs SCE) and potential was stepped in positive direction with step of 0.1 V as explained in chapter 4.

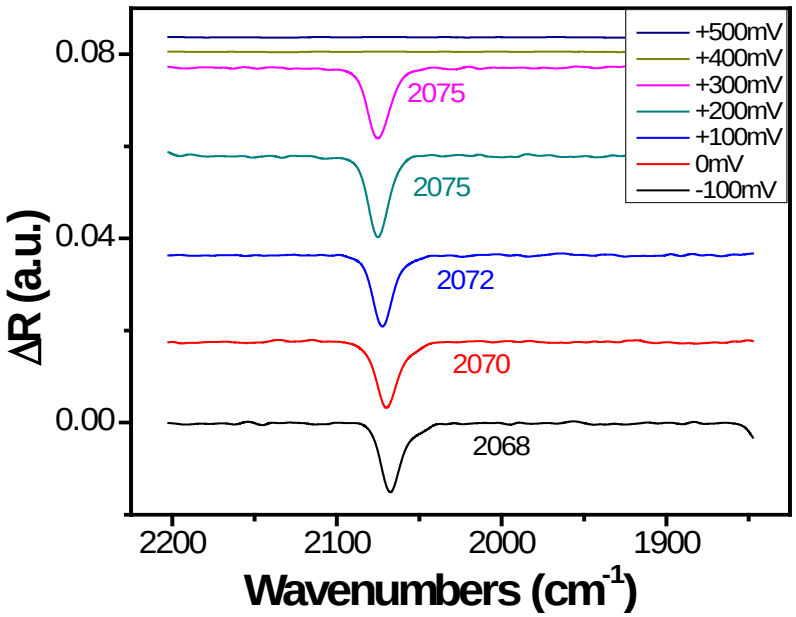

Figure **5-4-1-1.** SNIFTIRS spectra for Pt(111) electrode in CO-saturated 0.1 M $HClO_4$. CO admission potential: - 0.1 V, reference: 0.9 V *vs.* to SCE.

Characteristic infrared wavenumbers (frequencies) (~2070 cm^{-1}) correspond to linearly adsorbed CO (CO_L) in saturated acid solution [36]. The variation of the band frequency maximum with applied potential is due to Stark effect [37,38] (chapter 4). The calculated slope value for CO IR peak position wavenumber dependence of potential (Figure 5-4-1-2) for this electrode is 25 $cm^{-1}V^{-1}$ which is consistent with the literature data (~30 $cm^{-1}V^{-1}$) [38,39].

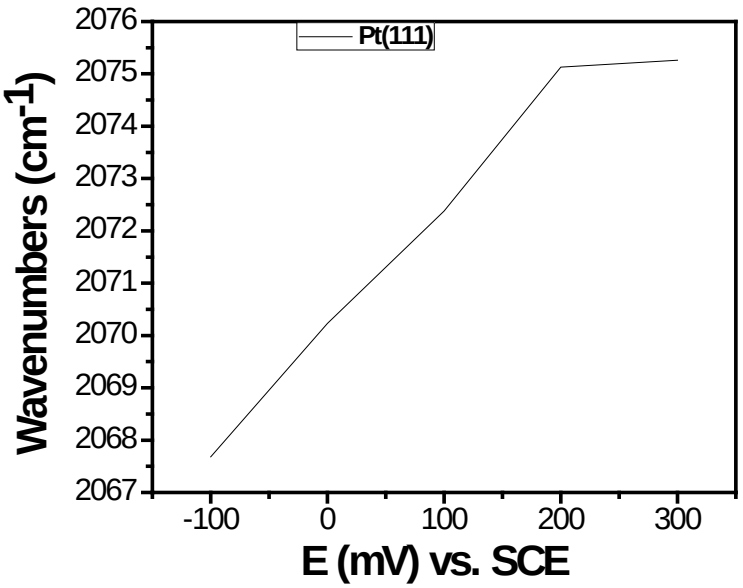

Figure 5-4-1-2. Potential dependence of the band maximum frequency for adsorbed CO on a Pt(111); slope dν/dE = 25 $cm^{-1}V^{-1}$.

Firstly, an increase of frequency i.e., increase of C-O bond strength at lower potentials is observed. Then, at higher potentials (i.e., 300 mV) the decrease of frequency and smaller band frequency shift step occurs due to coverage dependence and anion co-adsorption. Namely, at certain potentials CO oxidation starts which leads to phase transformation of the remaining CO giving adequate response in the frequency of the band maximum. Furthermore, by increasing the potential, the CO will be totally oxidized and no spectra

will be observed with SNIFTIRS (Figure 5-1-4-1 at 400 mV and 500 mV). In the Figure 5-4-1-3 the *i-V* transients are shown, after linear stripping voltammetry (LSV) of adsorbed CO is performed in the acid solution saturated with CO. The sharp increase of the current corresponds to the onset of CO oxidation, followed by full oxidation of the adsorbed CO. This LSV data are in agreement with IR spectra.

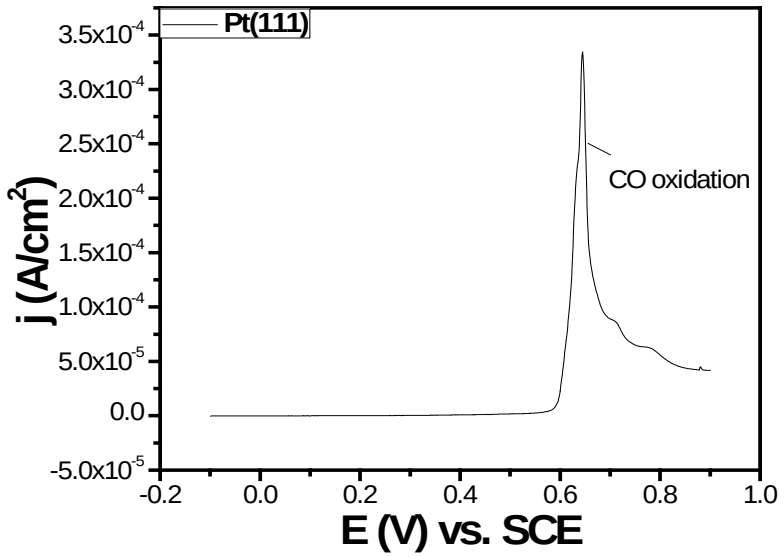

Figure 5-4-1-4. LSV transients for a Pt(111) electrode of CO saturated 0.1 M $HClO_4$ solution.

Pd(111)

The same type of data are obtained for Pd single crystal with (111) surface orientation. The two kinds of absorption bands of CO on the Pd(111) electrode surface, are assignable to CO stretch vibration bands in two-fold and three-fold hollow sites [40] (Figure 5-4-1-5).

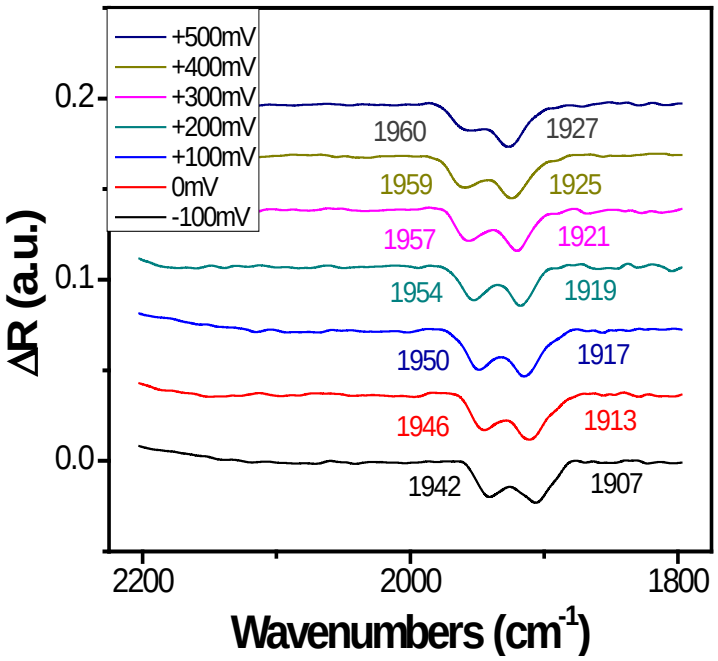

Figure 5-4-1-5. CO adsorption SNIFTIRS spectra for Pd(111) in 0.1 M $HClO_4$ solution. Potentials are referred to SCE.

The calculated slope of peak position vs. potential for the peak at higher frequency (Figure 5-4-1-6 (a)) is 37 $cm^{-1}V^{-1}$ is in agreement with literature for this metal surface [38,39]. Also, corresponding CO oxidation LSV graph is obtained for this surface (Figure 5-4-1-6 (b). The oxidation of CO on Pd(111) starts at 0.1 V more positive than on Pt(111), in accordance with stronger M-CO bond on Pd than on Pt observed by SNIFTIRS.

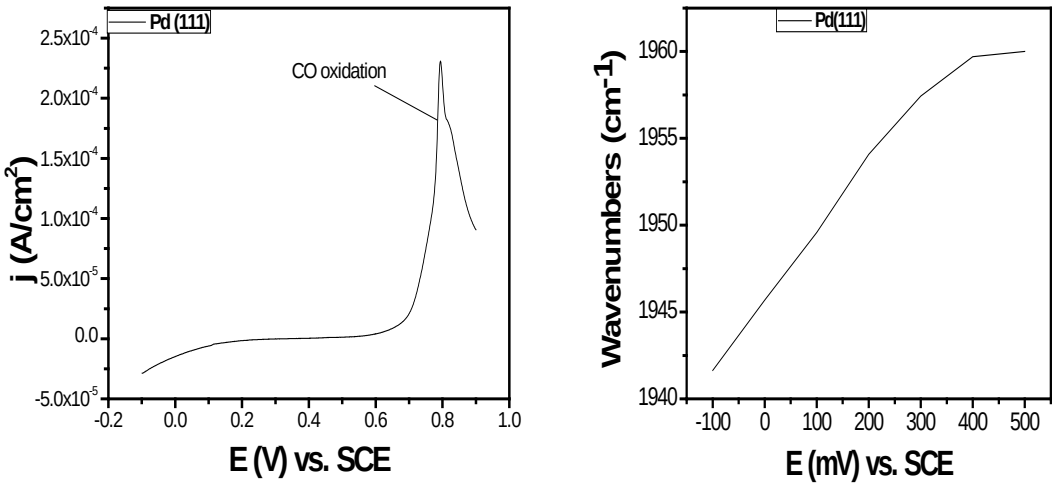

(a) (b)

Figure 5-4-1-6. Plots of CO oxidation (a) and of CO IR peak position wavenumber vs. potential (b) for Pd(111) in 0.1 M $HClO_4$; slope $d\nu/dE = 30\ cm^{-1}V^{-1}$.

Pt modified Pd(111) without citrate (Pt_{ML}/Pd(111) w/oc)

The modification of Pd(111) by Pt_{ML} is done by SLRR of an UPD previously described in the chapter 4. The formed Pt monolayer is then characterized by cyclic voltammetry (chapter 5) as well as SNIFTIRS technique. The obtained SNIFTIRS data, for the surface formed without presence of citrate ions during synthesis of Pt_{ML}, are presented in the Figure 5-4-1-7.

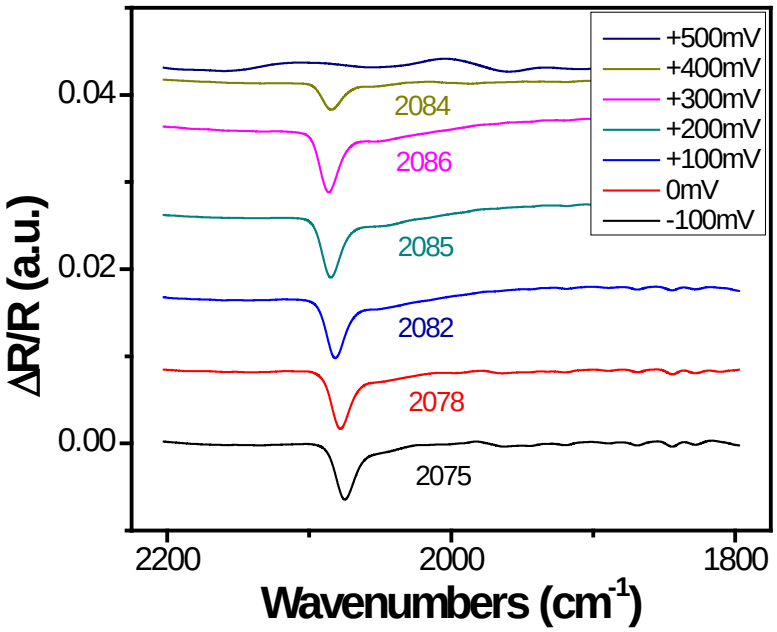

Figure 5-4-1-7. SNIFTIRS spectra for Pt modified Pd(111) electrode without citrate, in CO-saturated 0.1 M $HClO_4$. CO admission potential: - 0.1 V, reference: 0.9 V *vs*. SCE.

After increase of the wavenumbers of the adsorption band with increase of potential, the peak at 400 mV decreases in its frequency due to CO partially oxidation and relaxation. Also, the peak at 500 mV is not observed. This is related to total oxidation of the CO so the subtraction and normalization of the interferogram from this potential with interferogram from reference potential gives no difference. The shift of the peak position frequency with change in potential for this surface is presented in the Figure 5-4-1-8 and measured to be the 30 $cm^{-1}V^{-1}$ slope.

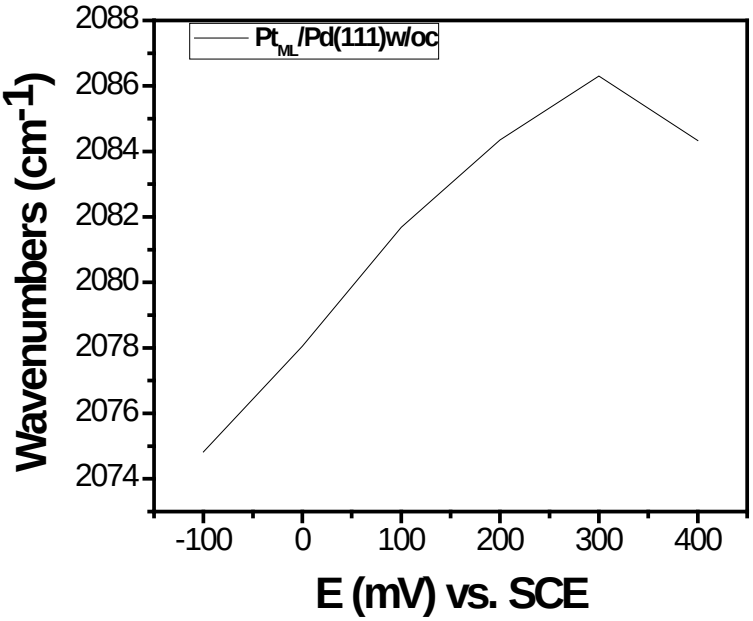

Figure 5-4-1-8. Potential dependence of the band maximum frequency for adsorbed CO on a Pt modified Pd(111) without citrate; $d\nu/dE = 30\ cm^{-1}V^{-1}$.

The SNIFTIRS data indicate that CO on Pt_{ML}/Pd(111) is bonded more weakly than on Pt(111) and Pd(111). This is a qualitatively new effect produced by synergy between Pt_{ML} and underlying Pd(111).

Pt modified Pd(111) synthesized with citrate (Pt_{ML}/Pd(111)wc)

The electrolyte design with citrate ions in solution for SLRR of Cu UPD is used for modifying Pd(111) surface with Pt_{ML} (chapter 4). The SNIFTIRS results are shown in Figure 5-4-1-9. As in previous case Pt_{ML}/Pd(111) has a weaker bond to CO than either Pd(111) or Pt(111) surface. Frequency shift vs. potential is 34 $cm^{-1}V^{-1}$ which is higher than on Pt and Pd surface indicating a weaker bond to Pt_{ML}/Pd(111) surface (Figure 5-4-1-10).

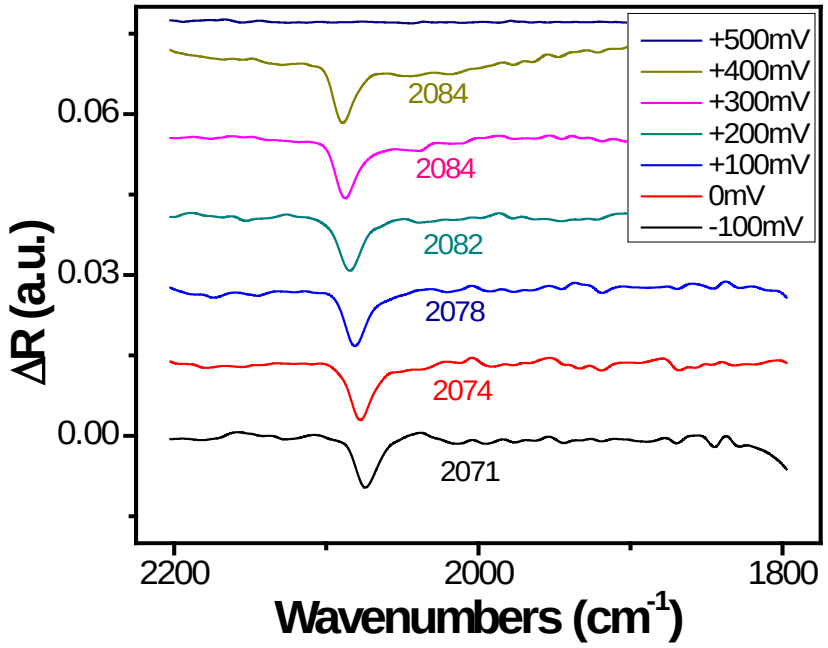

Figure 5-4-1-9. SNIFTIRS spectra for Pt_{ML}/Pd(111) electrode synthesized with citrate, in CO-saturated 0.1 M $HClO_4$. CO admission potential: - 0.1 V, reference: 0.9 V *vs.* to SCE.

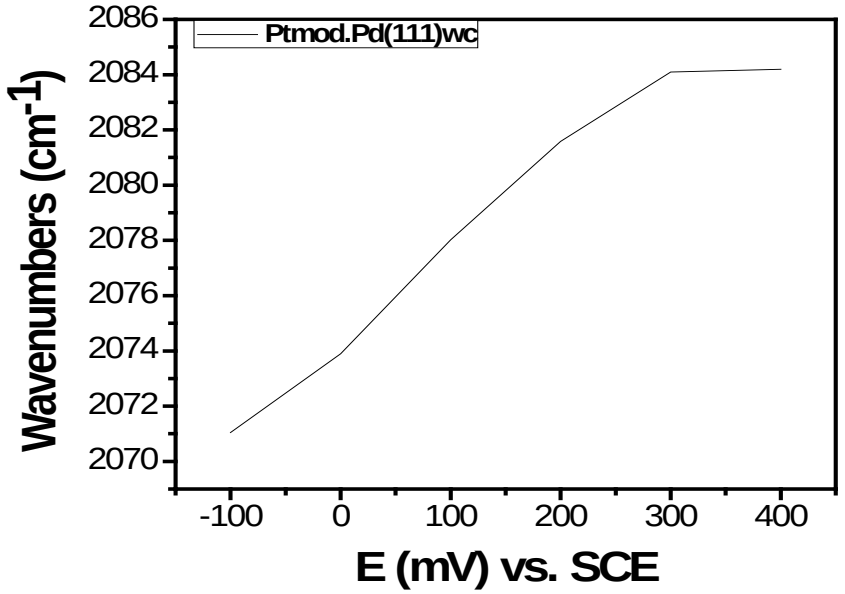

Figure 5-4-1-10. Potential dependence of the band maximum frequency for adsorbed CO on a Pt modified Pd(111) synthesized with citrate; dv/dE = 34 $cm^{-1}V^{-1}$.

5.4.2. The (100) Plane orientation

Pt(100)

The spectra of the linearly adsorbed CO on the Pt(100) surfaces at different potentials are presented in graph 5-4-2-1. The obtained frequencies are in agreement with the literature data [41]. The calculated slope for the frequency shift vs. potential plot (Figure 5-4-2-2 (a)) is 27 $cm^{-1}V^{-1}$. The oxidation of CO on this surface is measured by linear stripping voltammetry in the solution saturated with CO (Figure 5-4-2-2 (b)). The LSV and IR data are in agreement indicating reduced CO presence/oxidation on Pt(100) at potentials more positive than 500mV *vs.* SCE.

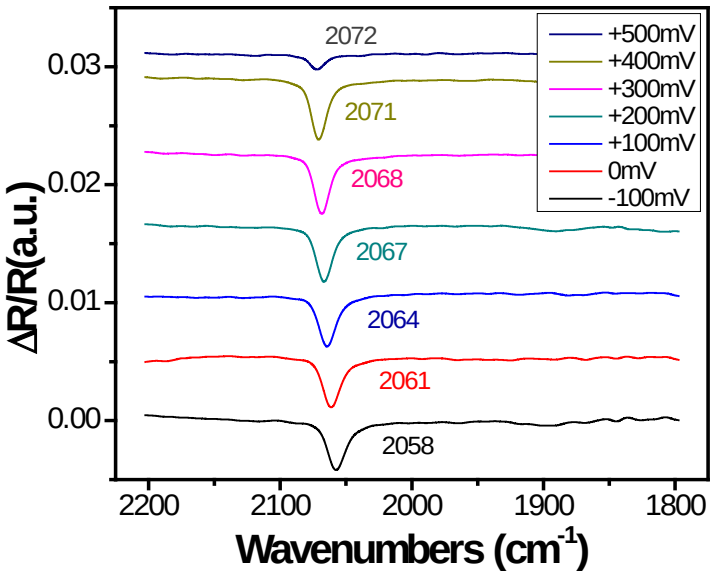

Figure 5-4-2-1. CO adsorption SNIFTIRS spectra for Pt(100) in 0.1 M $HClO_4$ solution. Potential is referred to SCE.

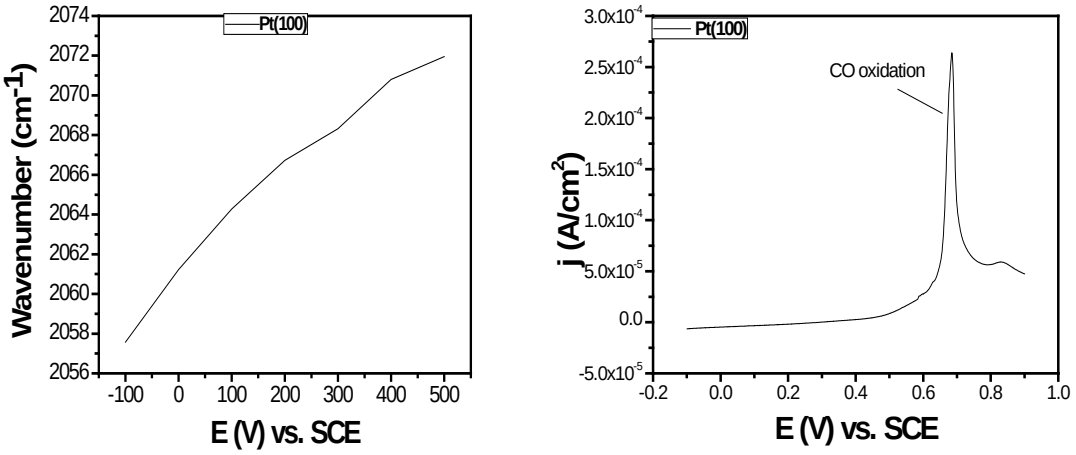

(a) (b)

Figure 5-4-2-2. Plots of CO IR peak position wavenumber vs. potential (a) and CO oxidation (b) for Pt(100) in 0.1 M $HClO_4$ *vs.* SCE; $d\nu/dE = 33\ cm^{-1}V^{-1}$.

Pd(100)

The same experiments are performed for Pd single crystal with (100) surface orientation. The absorption bands of CO on the Pd(100) electrode surface is assignable to CO linearly bonded [40] (Figure 5-4-2-3). The calculated slope of peak position vs. potential for the peak at higher frequency (Figure 5-4-2-4 (a)) is 30 $cm^{-1}V^{-1}$ is in agreement with literature for this metal surface. Also, corresponding LSV of CO oxidation graph is obtained for this surface (Figure 5-4-2-4 (b)).

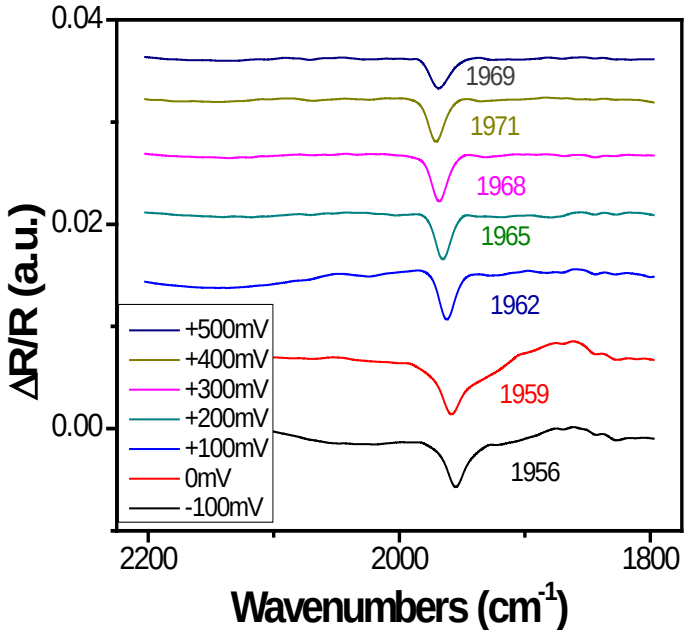

Figure 5-4-2-3. CO adsorption SNIFTIRS spectra for Pd(100) in 0.1 M $HClO_4$ solution. Potential presented *vs.* SCE.

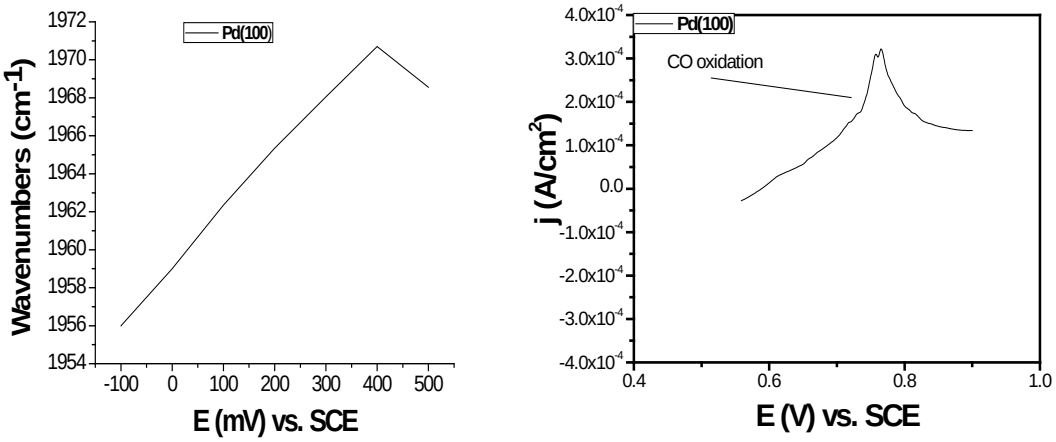

(a) (b)

Figure 5-4-2-4. Plots of CO IR peak position wavenumber vs. potential (a) and CO oxidation (b) for Pd(100) in 0.1 M $HClO_4$; dv/dE = 30 $cm^{-1}V^{-1}$.

Pt modified Pd(100) without citrate (Pt_{ML}/Pd(100) w/oc)

The obtained SNIFTIRS data, for the surface formed without presence of citrate ions during synthesis of Pt_{ML}/Pd(100) are presented in the Figure 5-4-2-5

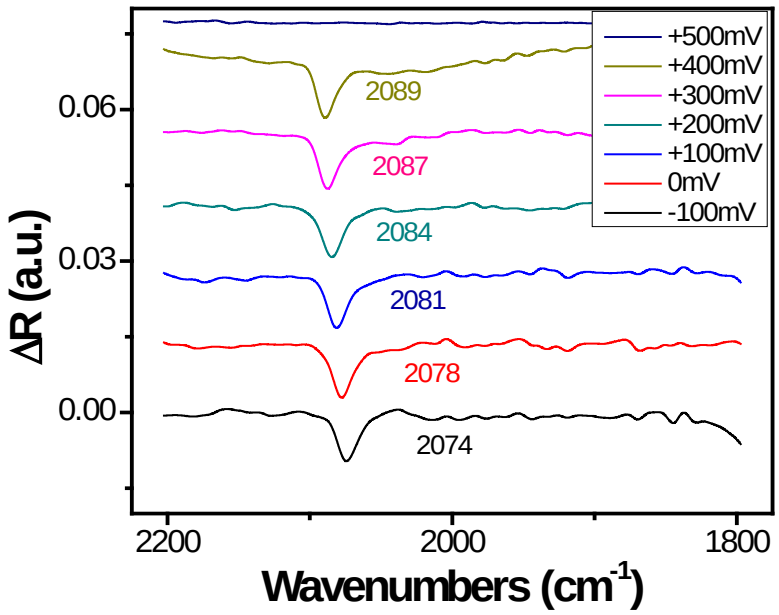

Figure 5-4-2-5. SNIFTIRS spectra for Pt modified Pd(100) electrode without citrate, in CO-saturated 0.1 M $HClO_4$. CO admission potential: - 0.1 V, reference: 0.9 V *vs.* SCE.

The SNIFTIRS data indicate that CO on Pt_{ML}/Pd(100) is bonded more weakly than on Pt(100) and Pd(100) which is in correlation with the data from Pt_{ML}/Pd(111) system. The shift is more pronounced in the case of (100) orientation.

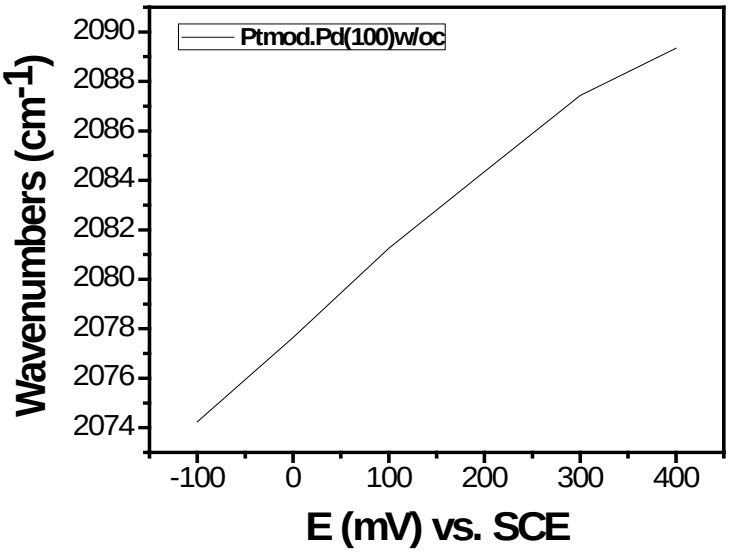

Figure 5-4-2-6. Potential dependence of the band maximum frequency for adsorbed CO on a Pt modified Pd(100) synthesized without citrate; dv/dE = 33 $cm^{-1}V^{-1}$.

Furthermore, wavenumber (frequency) shift vs. potential is 33 $cm^{-1}V^{-1}$ which is higher than on Pt and Pd surface indicating a weaker bond to Pt_{ML}/Pd(100) surface (Figure 5-4-2-6). This tuning rate is the same as for Pt_{ML}/Pd(111) surface.

Pt modified Pd(100) with citrate (Pt_{ML}/Pd(100)wc)

The SNIFTIRS spectra in the Figure 5-4-2-7 show the big increase in the wavenumbers of adsorbed CO vibration bands for the surface formed with presence of citrate ions during synthesis of Pt_{ML}/Pd(100).

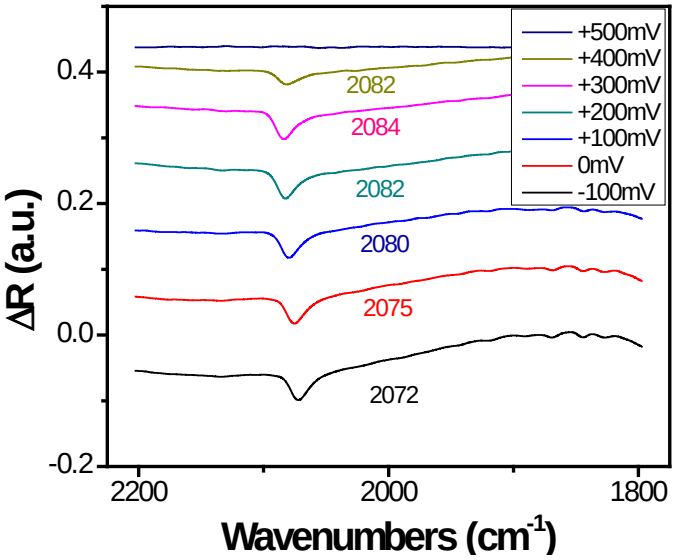

Figure 5-4-2-7. SNIFTIRS spectra for Pt modified Pd(100) electrode with citrate, in CO-saturated 0.1 M $HClO_4$. CO admission potential: - 0.1 V, reference: 0.9 V *vs.* SCE.

Wavenumbers (frequency) shift vs. potential is 35 $cm^{-1}V^{-1}$.

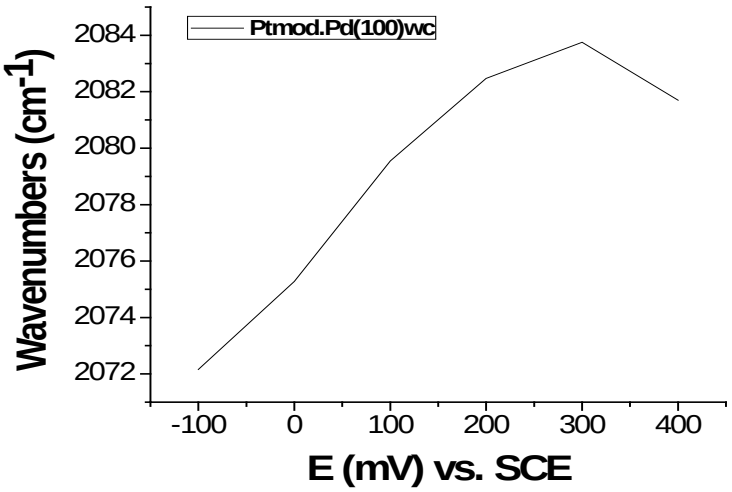

Figure 5-4-2-8. Potential dependence of the band maximum frequency for adsorbed CO on a Pt modified Pd(100) with citrate; dν/dE = 35 $cm^{-1}V^{-1}$.

5.4.3. Comparison Pt_{ML}/Pd(hkl) CO adsorption with Pt(hkl) and Pd(hkl) surfaces

The altered behavior of the modified surfaces can be represented straightforwardly by plotting the spectra of CO adsorption on specific potential (i.e., 100 mV) and comparing the wavenumbers of band maximum.

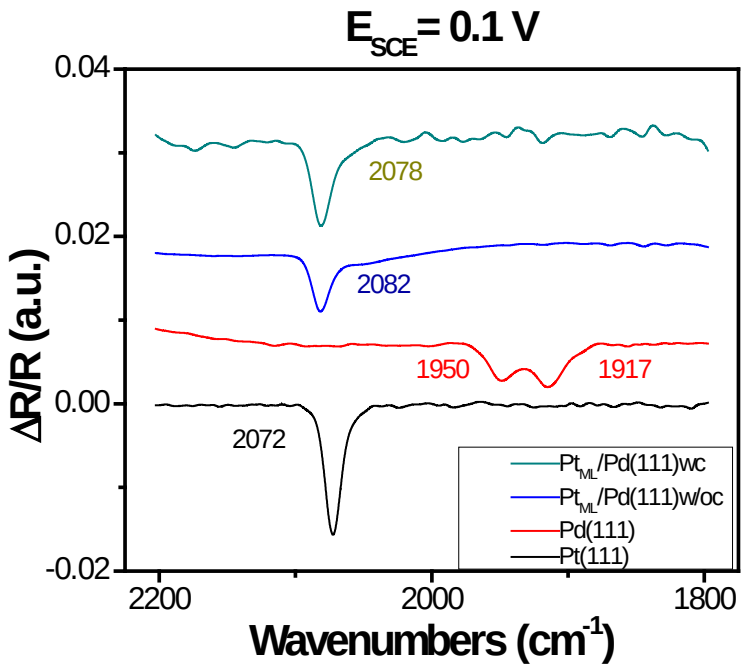

Figure 5-4-3-1. Comparison of the SNIFTIRS spectra for the different (111) surfaces on the same potential (100 mV *vs.* SCE).

The obtained graph for the (111) system showed distinct frequency features (Figure 5-4-3-1). Single crystals Pt and Pd with CO adsorption band frequencies at 2072 cm^{-1} and 1950 cm^{-1} (1^{st} peak) are compared with Pt_{ML}/Pd(111) synthesized with (2078 cm^{-1}) and without (2082 cm^{-1}) citrate. Furthermore, the noticeable difference between Pt_{ML}/Pd(111) prepared with citrate in the solution and Pt_{ML}/Pd(111) without citrate is observed. This difference is confirmed with the series of experiments. The overall representation of the differences between surfaces is shown in the Figure 5-4-3-2. The

band maximums at each potential for the (111) surfaces are plotted together. The band maximum frequency indicates susceptibility for particular surface to bind CO, i.e., higher frequency on the graph stronger C-O bond i.e. weaker C-substrate bond and *vice versa*.

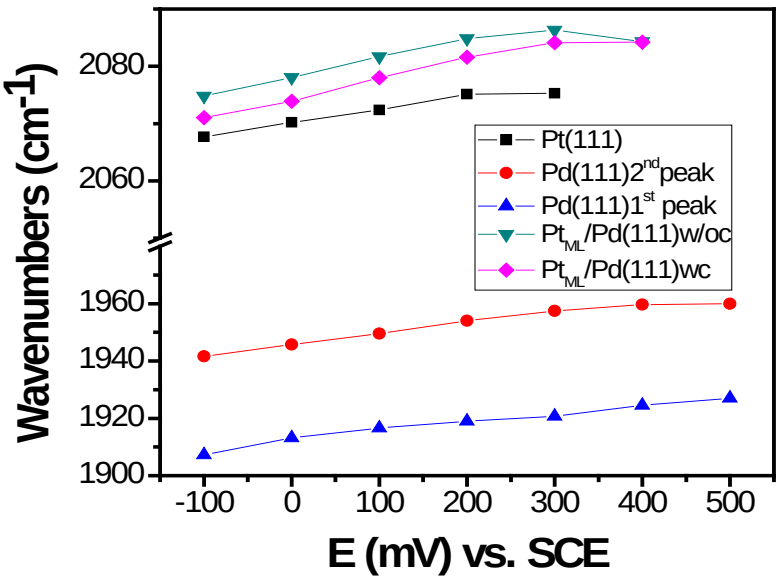

Figure 5-4-3-2. Plots of CO SNIFTIRS peak position wavenumber *vs.* potential for different surfaces with (111) plane orientation.

The similar graphs are obtained for (100) surfaces. The potential where the frequency wavenumber decreases (decreasing peak) is in good agreement with the CO oxidation from LSV. Comparing the position of the decreasing peak for different surfaces the conclusion can be made of the onset of oxidation i.e. susceptibility of the surface for oxidation of particular molecule (CO).

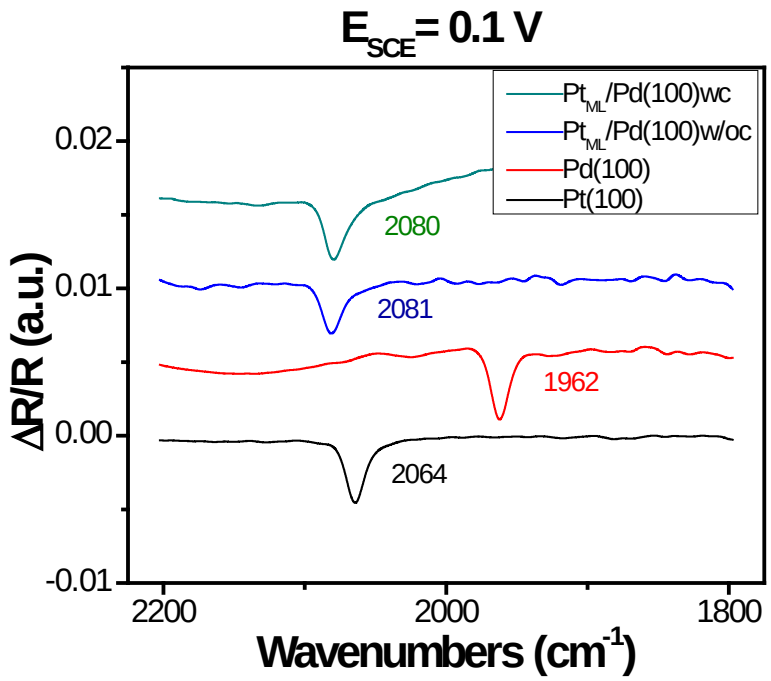

Figure 5-4-3-3. The comparison of SNIFTIRS spectra for different (100) surfaces on the same potential (100 mV *vs.* SCE).

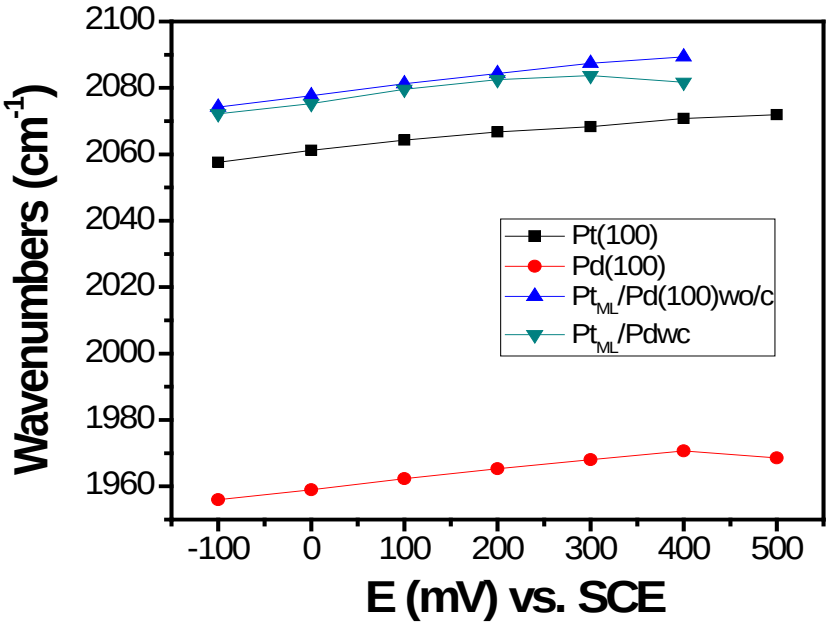

Figure 5-4-3-4. Plots of CO SNIFTIRS peak position wavenumber *vs.* potential for different surfaces with (100) plane orientation.

CHAPTER 6: CONCLUSIONS AND FUTURE WORK

The interest for a new energy sources propelled the research in the fuel cells. The needs for better catalyst initiated the development of several techniques for design and manufacture of novel electrode catalyst materials. The electrochemical deposition technique, demonstrated by deposition of a monolayer of Pt on the Pd(hkl) surfaces by using a Cu adlayer as a sacrificial template, was found practical and effective. The deposition of a noble metal occurs as an irreversible surface redox reaction. In the first part of this work, the presented results and discussions address the details of Pt redox replacement of the Cu(UPD)/Pd(hkl) . The Pt_{ML}/Pd(hkl) formation is verified by series of cyclic voltammetry and STM measurements. The effect of citrate ions in the solution during the redox process is also investigated. The Pt_{ML} surface synthesized with or without citrate showed different electrochemical behavior towards adsorption and desorption of ions (bisulphate) as absence of the substrate (Pd) oxide formation. Also, the Pt oxidation and reduction is altered. The morphology of the deposits is investigated with STM technique. The STM images of the Pt_{ML}/Pd(hkl) surface synthesized with citrate showed morphology with 2D morphology with the Pt clusters uniformly deposited. The STM images confirmed the formation of the Pt layer and gave qualitative comparison of two modified surfaces.

The SNIFTIRS, as main technique in this work, was used to probe the affinity of synthesized Pt_{ML}/Pd(hkl) towards molecule bonding and CO oxidation processes. The electrocatalytic activity of the electrodes used in fuel cells can be blocked by intermediates. In the oxygen reduction reaction active sites on the cathode are poisoned by OH ions and when organic molecules (methanol, ethanol) are used the CO

(intermediate) is bonding strongly on the surface decreasing activity of the cathode. The CO is used as a probe molecule in this research due to its ability to easily bond on the Pt, pronounced Stark effect, and of his importance being most common intermediates when organic molecules are oxidized as a fuel in fuel cells. Therefore, the SNIFTIRS is employed to investigate the CO-bond strength and electrocatalytic activity of Pt monolayer supported by Pd(hkl) substrates. The results on the modified electrodes shows the IR spectra with band maximums shifted towards the higher frequencies than one expects from comparison to the wavenumbers of the adsorbed CO on Pt and Pd single crystals. Comparing two orientation of substrate surfaces, (111) and (100), resulted in more pronounced shift with (100) surface orientation. Also, the comparison of two synthetic routes for Pt_{ML}/Pd(hkl) formation (with or without citrate) the more pronounced shift is in the case of the surface synthetized without citrate and again, the higher discrepancy is at the (100) surface orientation. The high wavenumbers of the adsorbed CO on the Pt_{ML}/Pd(hkl) means stronger C-O bond and weaker the C-metal bond. The bonding strength should be optimized for higher adsorption of reactive molecules and weaker adsorption of intermediates. The substrate effect is verified on this Pt-Pd model. To clarify the type of the effect of the substrate (electronic or strain) the different substrate can be used in the future work. The Pd(hkl) replacement with the Au(hkl) as a substrate should give more information of the ligand (electronic) effect considering Au(hkl) as substrate with the poor ligand abilities. Therefore, the difference could be made and possible size effect will be confirmed or excluded.

REFERENCES

1. B.C. Gates, Catalytic chemistry, Wiley (1992).

2. R.A. van Santen, M. Neurock, Molecular Heterogeneous Catalysis, Wiley-VCH (2006), p. 22.

3. J. K. Nørskov, J. Rossmeisl, A. Logadottir, L. Lindqvist, J. R. Kitchin, T. Bligaard and H. Jónsson, "Origin of the Overpotential for Oxygen Reduction at a Fuel-Cell Cathode."J. Phys. Chem. B, 108, 17886 (2004).

4. T. Toda, H. Igarashi,M. J.Watanabe, "Enhancement of the electrocatalytic O2 reduction on Pt-Fe alloys."Electroanal. Chem., 460, 258(1999).

5. S.R. Brankovic, J.X. Wang, R.R. Adzic, "Metal monolayer deposition by replacement of metal adlayers on electrode surfaces."Surface Science, 474 (2001).

6. J. Lipkowski, P. N. Ross, Electrocatalysis, Wiley-VCH (1998), p. 44-57.

7. A. Wieckowski, Catalysis in Electrochemistry, Wiley (2011), p. 297.

8. R. J. H. Clark, R. E. Hester, Spectroscopy for Surface Science, Wiley (1998), p. 274.

9. A. Berna, A. Rodes, J.M. Feliu, *Electrochim. Acta*49 (2004) 1257.

10. D. Kardash, C. Korzeniewski, N. Markovic, *J. Electroanal. Chem.* 500 (2001) 518.

11. S. Park, A. Wieckowski, M. J. Weaver, *J. Am. Soc.* 125 (2003) 2282.

12. C. Korzeniewski, D. Snow, R. Basnayake, *Appl. Spectrosc.* (2006) 599.

13. J. S. E. Lipkowski, *J. Electroanal. Chem.* 550-551 (2002).

14. S. G. Sun, P. A. Christensen, A. Wieckowski, In-situ Spectroscopic Studies of Adsorption at the Electrode and Electrocatalysis, Elsevier (2007) p. 1.

15.W.G. Golden, D.S. Dunn and J. Overend, *J. Catal.*71 (1981) 395.

16. B. Pettinger, J. Lipkowski, M.Hoon-Khosla, "Simulation of SNIFTIRS experiments."

17. D. J. O'Connor, B. A. Sexton. R. St. C. Smart, Surface Analysis Methods in Materials Science, Springer-Verlag (1992) p. 192.

18. R. C. Alkire, D. M. Kolb, J. Lipkowski, Electrochemical Surface Modification, Wiley-VCH (2008).

19. D. Gokcen, S.-E. Bae, S.R. Brankovic, "Reaction kinetics of Metal depostion via surface limited red-ox replacement of underpotentially deposited metal monolayers," *ElectrochimicaActa*, 56, 5545 (2011).

20. S. G. Corcoran, G. S. Chakarova, and K. Sieradzki, "An In Situ Investigation of Underpotential Deposition of Ag on Au(111) Electrode," *J. Electranal. Chem.* 377, 85 (1994).

21. E. Budevski, G. Staikov and W. J. Lorenz in Electrochemical Phase Formation and Growth, ed. R.C. Alkire*et al*. VCH, Berlin (1996).

22. S. R. Brankovic, in Functional Properties of Bioinspired Surfaces – Properties and Technological Application, ed. E. Favret and N. Fuentes, World Scientific, Singapore (2009).

23. J. L. Znahg, M.B. Vukmirovic, K. Sasaki, A. U. Nilekar, M. Marvikakis, R. R. Adzic, "Mixed Monolayer Electrocatalysts for Enhanced Oxygen Reduction Kinetics," *J. Am. Chem. Soc.*, 127, 12480 (2005).

24. L. T. Viyannaiage, R. Vasilic, and N. Dimitrov, "Epitaxial growth of Cu on Au(111) and Ag(111) by surface limited redox replacement - An electrochemical and STM study," *J. Phys. Chem.* ***C***, 111, 4036 (2007).

25. J. Clavilier, *J. Electroanal. Chem.*, 107 (1980) 211.

26. K. Al Jaaf-Golze, D.M. Kolb, D. Scherson, "On the Voltammetry Curves of Pt (111) in Aqueous Solutions," *J.Electroanal. Chem.*, 200 (7986) 353-362.

27. A.Zolfaghari, G.Jerkiewicz, "Temperature-dependent research on Pt(111) and Pt(100) electrodes in aqueous H_2SO_4," *Journal of Electroanalytical Chemistry* 467 (1999) 177–185.

28. E.Herrero, J. Mostany, J. M. Feliu, J.Lipkowski, "Thermodynamic studies of anion adsorption at the Pt(111) electrode surface in sulfuric acid solutions," *Journal of Electroanalytical Chemistry* 534 (2002) 79/89.

29. J.Inukai, M. Ito, "Electrodeposition processes of palladium and rhodiummonolayers on Pt(111) and Pt(100) electrodes studied byIR reflection absorption spectroscopy," *J. Electroanal. Chem.*, 358 (1993) 307-315.

30. V. D. Colle, M. J. Giz, G.Tremiliosi-Filho, "Spontaneous deposition of Ru on Pt (100): morphological and electrochemical studies. Preliminary results of ethanol oxidation at Pt(100)/Ru," *J. Braz. Chem. Soc*. vol.14 no.4 (2003).

31. J. Inukai, M. Ito, "Electrodeposition processes of palladium and rhodium monolayers on Pt(111) and Pt(100) electrodes studied by IR reflection absorption spectroscopy," *J.Electroanal. Chem.*, 358 (1993) 307-315.

32. J. Okada, J. Inukai, K. Itaya, “Underpotential and bulk deposition of copper on Pd(111) in sulfuric acid solution studied by in situ scanning tunneling microscopy,” *Phys. Chem. Chem. Phys*., (2001).

33. J. Zhang, Y. Mo, M. B. Vukmirovic, R. Klie, K. Sasaki, R. R. Adzic, “PlatinumMonolayer Electrocatalysts for O_2 Reduction: Pt Monolayer on Pd(111) and onCarbon-Supported Pd Nanoparticles,”*J. Phys. Chem.B* 2004, 108, 10955-10964.

34. L. Fang, Q. Tao, M. Li, L. Liao, D. Chen, Y. Chen, “Determination of the Real Surface Area of Palladium Electrode,” *Chinese Journal of Chem. Phys*. vol. 23, (2010) .

35. P. M. Rigano, C. Mayer, T. Chierciue, “Structural Investigation of the Initial Stages of Copper Electrodeposition on Polycrystalline and Single Crystal Palladium Electrodes,” *Electrochimica Acta*, Vol. 35, No. 7, pp. 1189-I 194, (1990).

36. S. Sun, P. A. Christensen, A. Wieckowski, In-situ Spectroscopy Studies of Adsorption at the Electrode and Electrocatalysis, Elsevier, (2007), p. 37.

37. S.Holloway, J.K. Worskow, *J. Electroanal. Chem.* 101, 193 (1984).

38. N.K. Ray, A.B. Anderson, *J. Phys. Chem.* 86, 4851 (1982).

39. S. Chang, M.J. Weaver, *Surf. Sci*. 230, 222 (1990).

40. K. Yoshioka, F. Kitamura, M. Takeda, M. Takahashi, M. Ito, “ Infrared Reflection Absorption Spectra of Carbon Monoxide Adsorbed on Single Crystal Electrodes, Pd (111) and Pd (100),” *Surface Science* 227 (1990).

41. S. Chang, M. J. Weaver, ”In situ infrared spectroscopy of carbon monoxide adsorbed at ordered platinum(100)-aqueous interfaces: double-layer effects upon the adsorbate binding geometry,” *J. Phys. Chem.*, 1990, 94 (12), pp 5095–5102.